TITLE:

# Influence of contamination on banded iron formations in the Isua supracrustal belt, West Greenland: Reevaluation of the Eoarchean seawater compositions

AUTHOR(S):

Aoki, Shogo; Kabashima, Chiho; Kato, Yasuhiro; Hirata, Takafumi; Komiya, Tsuyoshi

CITATION:

Aoki, Shogo ...[et al]. Influence of contamination on banded iron formations in the Isua supracrustal belt, West Greenland: Reevaluation of the Eoarchean seawater compositions. Geoscience Frontiers 2018, 9(4): 1049-1072

ISSUE DATE:

2018-07

URL:

http://hdl.handle.net/2433/232945

RIGHT:

© 2017, China University of Geosciences (Beijing) and Peking University. Production and hosting by Elsevier B.V. This is an open access article under the CC BY-NC-ND license (http://creativecommons.org/licenses/by-nc-nd/4.0/).

京都大学学術情報リポジトリ
KURENAI 紅
Kyoto University Research Information Repository

京都大学 KYOTO UNIVERSITY
A Self-archived copy in
Kyoto University Research Information Repository
https://repository.kulib.kyoto-u.ac.jp
京都大学学術情報リポジトリ KURENAI 紅 Kyoto University Research Information Repository

Geoscience Frontiers 9 (2018) 1049–1072

HOSTED BY

ELSEVIER

Contents lists available at ScienceDirect

China University of Geosciences (Beijing)

Geoscience Frontiers

journal homepage: www.elsevier.com/locate/gsf


Research Paper

# Influence of contamination on banded iron formations in the Isua supracrustal belt, West Greenland: Reevaluation of the Eoarchean seawater compositions

Shogo Aoki [a,*], Chiho Kabashima [b], Yasuhiro Kato [b,c,d,e], Takafumi Hirata [f], Tsuyoshi Komiya [a]

[a] Department of Earth Science and Astronomy, The University of Tokyo, 3-8-1 Komaba, Meguro-ku, Tokyo 153-8902, Japan
[b] Frontier Research Center for Energy and Resources, School of Engineering, The University of Tokyo, 7-3-1 Hongo, Bunkyo-ku, Tokyo 113-8656, Japan
[c] Department of Systems Innovation, School of Engineering, The University of Tokyo, 7-3-1 Hongo, Bunkyo-ku, Tokyo 113-8656, Japan
[d] Ocean Resources Research Center for Next Generation, Chiba Institute of Technology, 2-17-1 Tsudanuma, Narashino, Chiba 275-0016, Japan
[e] Research and Development Center for Submarine Resources, Japan Agency for Marine-Earth Science and Technology (JAMSTEC), 2-15 Natsushima, Yokosuka, Kanagawa 237-0061, Japan
[f] Division of Earth and Planetary Sciences, Kyoto University, Kitashirakawa Oiwake-cho, Sakyo-ku, Kyoto 606-8502, Japan

ARTICLE INFO

*Article history:*
Received 5 April 2016
Received in revised form
11 November 2016
Accepted 25 November 2016
Available online 11 January 2017

*Keywords:*
Banded iron formations
Eoarchean
Isua supracrustal belt
Bioessential elements
Seawater compositions

ABSTRACT

Banded Iron Formations (BIFs) are chemical sediments, ubiquitously distributed in the Precambrian supracrustal belts; thus their trace element compositions are helpful for deciphering geochemical evolution on the Earth through time. However, it is necessary to elucidate factors controlling the whole-rock compositions in order to decode the ancient seawater compositions because their compositions are highly variable. We analyzed major and trace element contents of the BIFs in the 3.8–3.7 Ga Isua supracrustal belt (ISB), southern West Greenland. The BIFs are petrographically classified into four types: Black-, Gray-, Green- and White-types, respectively. The Green-type BIFs contain more amphiboles, and are significantly enriched in Co, Ni, Cu, Zn, Y, heavy rare earth element (HREE) and U contents. However, their bulk compositions are not suitable for estimate of seawater composition because the enrichment was caused by secondary mobility of metamorphic Mg, Ca and Si-rich fluid, involvement of carbonate minerals and silicate minerals of olivine and pyroxene and/or later silicification or contamination of volcanic and clastic materials. The White-type BIFs are predominant in quartz, and have lower transition element and REE contents. The Gray-type BIFs contain both quartz and magnetite. The Black-type BIFs are dominated by magnetite, and contain moderate to high transition element and REE contents. But, positive correlations of V, Ni, Zn and U contents with Zr contents suggest that involvement of detrital, volcanic and exhalative materials influences on their contents. The evidence for significant influence of the materials on the transition element contents such as Ni in the BIFs indicates the transition element contents in the Archean ocean were much lower than previously estimated. We reconstructed secular variations of V, Co, Zn and U contents of BIFs through time, which show Ni and Co contents decreased whereas V, Zn and U contents increased through time. Especially, the Ni and Co contents drastically decreased in the Mesoarchean rather than around the Great Oxidation Event. On the other hand, the V, Zn and U contents progressively increased from the Mesoarchean to the Proterozoic. Stratigraphical trends of the BIFs show increase in Y/Ho ratios and decrease in positive Eu anomaly upwards, respectively. The stratigraphic changes indicate that a ratio of hydrothermal fluid to seawater component gradually decrease through the deposition, and support the Eoarchean plate tectonics, analogous to the their stratigraphic variations of seafloor metalliferous sediments at present and in the Mesoarchean.

© 2017, China University of Geosciences (Beijing) and Peking University. Production and hosting by Elsevier B.V. This is an open access article under the CC BY-NC-ND license (http://creativecommons.org/licenses/by-nc-nd/4.0/).

* Corresponding author.
*E-mail address:* shogo@ea.c.u-tokyo.ac.jp (S. Aoki).
Peer-review under responsibility of China University of Geosciences (Beijing).

http://dx.doi.org/10.1016/j.gsf.2016.11.016
1674-9871/© 2017, China University of Geosciences (Beijing) and Peking University. Production and hosting by Elsevier B.V. This is an open access article under the CC BY-NC-ND license (http://creativecommons.org/licenses/by-nc-nd/4.0/).

京都大学 KYOTO UNIVERSITY
A Self-archived copy in
Kyoto University Research Information Repository
https://repository.kulib.kyoto-u.ac.jp
京都大学学術情報リポジトリ KURENAI 紅 Kyoto University Research Information Repository



## 1. Introduction

Coevolution of the surface environment and life through time is one of the most significant features of the Earth. Decoding of ocean chemistry in the early Earth is a key issue to understand the origin and evolution of life, but it is difficult to directly estimate the composition because ancient seawater cannot be preserved. The geochemistry of banded iron formations (BIFs) provides one of the powerful proxies to estimate the ancient seawater because they ubiquitously occur in the Archean, and contain high abundances of transitional metals and rare earth elements (REEs). Their REE + Y patterns and trace element compositions (e.g. Ni, Cr, Co and U) are considered to be related with contemporaneous ocean chemistry (e.g. Bau and Dulski, 1996; Bau and Dulski, 1999; Bjerrum and

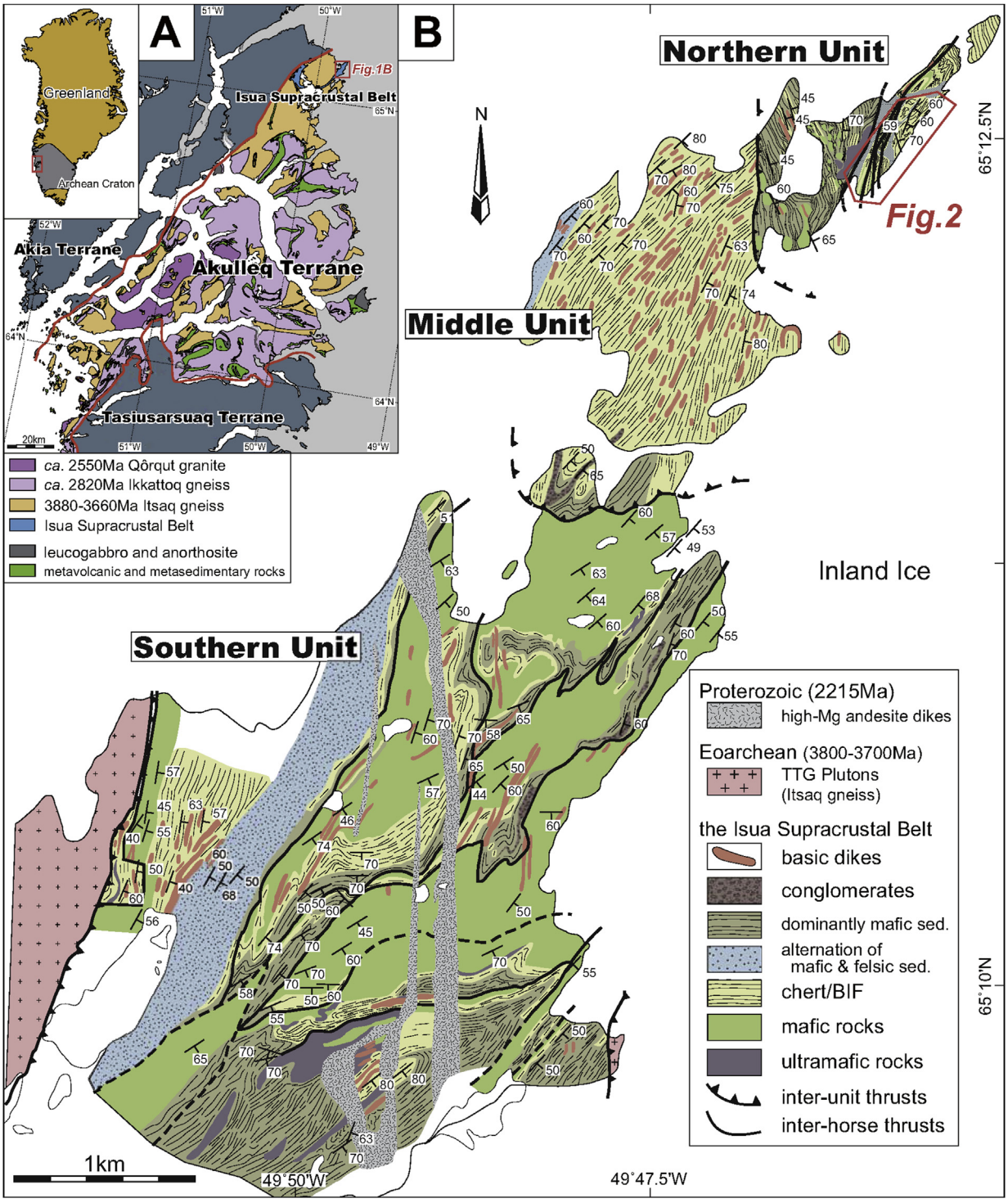


**Figure 1.** (A) A geological map of the Southern West Greenland, which comprises Akia, Akulleq and Tasiussarsuaq terranes. The Akulleq Terrane is composed of Ikkattoq gneiss, Amîtsoq gneiss, supracrustal rocks and post-collision Qôrqut granite, in the southern West Greenland (modified from McGregor, 1993). The Isua supracrustal belt (the ISB) is located in the northeastern part. (B) A geological map of the northeastern part of the Isua supracrustal belt (modified after Komiya et al., 1999). Our studied area is located in the northeastern part (Fig. 2).

A Self-archived copy in
Kyoto University Research Information Repository
https://repository.kulib.kyoto-u.ac.jp



Canfield, 2002; Bolhar et al., 2004; Konhauser et al., 2009, 2011; Partin et al., 2013; Swanner et al., 2014). Konhauser and his colleagues showed that the Archean BIFs have higher Ni/Fe ratios than post-Archean BIFs and iron-oxide deposits, and suggested that the Archean seawater was more enriched in Ni contents due to higher hydrothermal Ni influx from komatiites to ocean, resulting in prosperity of methanogens because Ni is an essential element to form Cofactor F430 (Konhauser et al., 2009; Pecoits et al., 2009; Mloszewska et al., 2012, 2013), which act as the enzyme catalyzing the release of methane in the final step of methanogenesis. However, the estimate is still controversial because the compiled Ni/Fe ratios of the BIFs are highly variable even in a single BIF

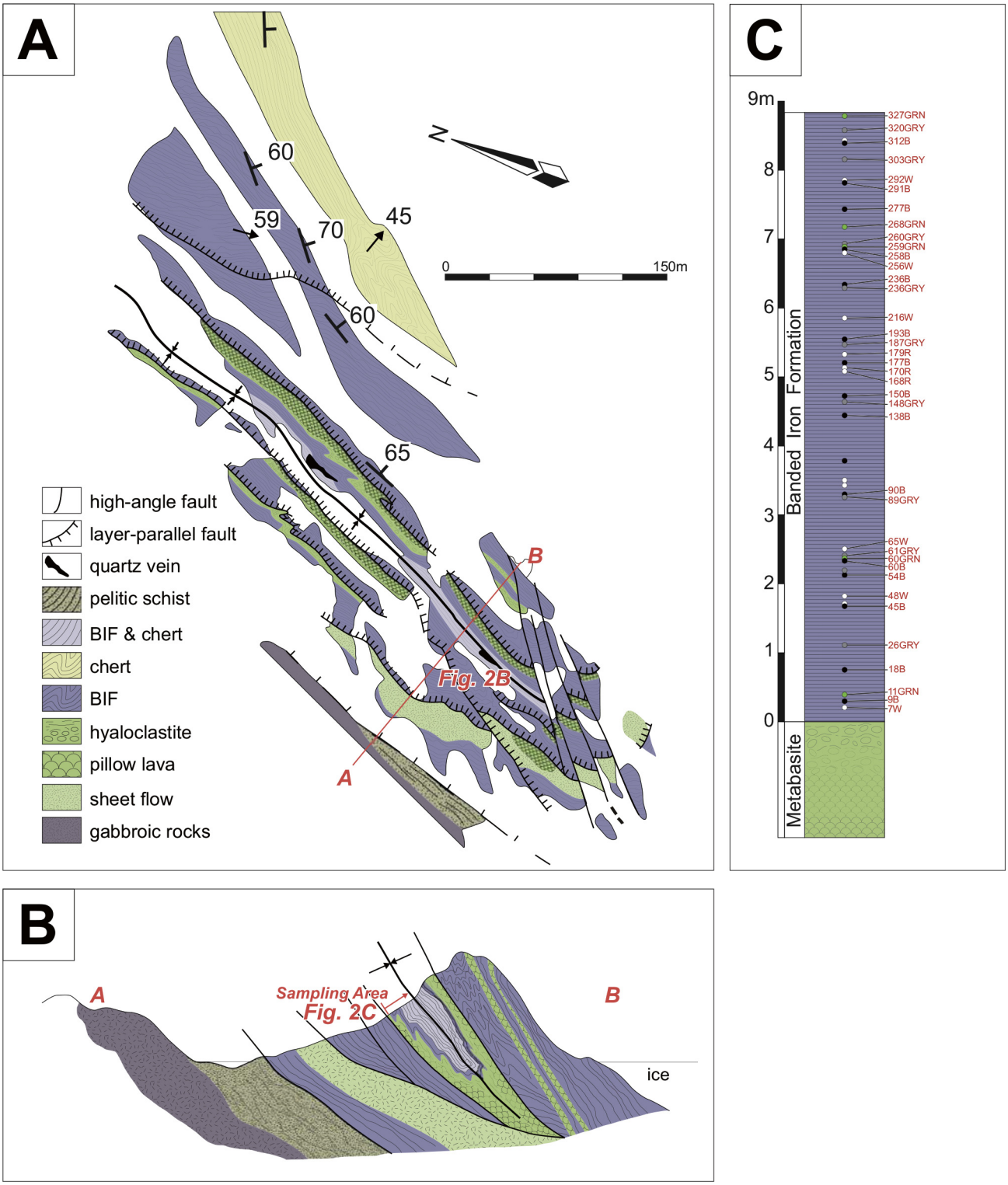


**Figure 2.** (A) A geological map of our studied area (modified after Komiya et al., 1999). (B) A cross section along A–B on Fig. 2A. (C) Stratigraphy and sample positions of the BIF sequence, which overlies basaltic hyaloclastite and pillow lavas.

京都大学 KYOTO UNIVERSITY
A Self-archived copy in
Kyoto University Research Information Repository
https://repository.kulib.kyoto-u.ac.jp
京都大学学術情報リポジトリ KURENAI 紅 Kyoto University Research Information Repository




**Figure 3.** The slabbed sections of BIF samples. (A) Alternation of black, white and gray bands, and (B) alternation of black and green bands. B: black band, W: white band, GRY: gray band, and GRN: green band.

sequence and because their chemical compositions are dependent on not only seawater composition but also various factors such as sedimentary rates (Kato et al., 1998, 2002), involvement of clastic and volcanic materials (Bau, 1993; Manikyamba et al., 1993; Frei and Polat, 2007; Pecoits et al., 2009; Viehmann et al., 2015a,b), secondary movement accompanied with metamorphism (Bau, 1993; Viehmann et al., 2015a,b) and kinetic of adsorption rates of the elements on the iron oxyhydroxides (Kato et al., 1998, 2002), other interference elements (Konhauser et al., 2009), and so on.

In general, the BIFs contain not only iron oxides (hematite and magnetite) and silica minerals (quartz), which are transformed from amorphous ferrihydrite and silica precipitated from seawater, but also carbonate and silicate minerals (Klein, 2005). The carbonate minerals are precipitated minerals from seawater or diagenetic minerals, and silicate minerals possibly originate from carbonate minerals precipitated from seawater, secondary minerals formed during diagenesis, metamorphism and alteration, and clastic and volcanic material. As a result, the whole-rock trace element compositions are dependent on not only compositions of the iron oxides and quartz but also those of other minerals. The most predominant minerals of the other silicate minerals are Mg- and Ca-bearing minerals such as amphibole and carbonate minerals (Dymek and Klein, 1988; Mloszewska et al., 2012, 2013). They have high REE and transition element contents but the effects of the involvement of the Mg- and Ca-bearing minerals on the whole rock compositions have not been fully evaluated yet.

The second component is derived from clastic and volcanic materials. They consist of clastic minerals such as detrital minerals of zircon, aluminosilicate minerals and quartz, aeolian dusts, and volcanic exhalative materials of tiny insoluble grains or colloidal particles. Some previous studies tried eliminating contamination of the clastic materials based on arbitrarily determined threshold values of some detritus-loving elements such as Al, Ti, Sc, Rb, Y, Zr, Hf and Th (e.g. Konhauser et al., 2009; Partin et al., 2013). However, even insignificant contaminations of clastic materials resulted in significant influence on the REE and transitional element compositions of the BIFs because they are much more abundant in clastic and exhalative materials relative to pure chemical sediments (Bolhar et al., 2004; Viehmann et al., 2015a,b), and are more abundant than the index elements of Zr, Y and Hf in most clastic and volcanic materials except for zircon. Therefore, it is necessary to more strictly eliminate the contaminations.

The 3.8–3.7 Ga Isua supracrustal belt (ISB) in southern West Greenland contains one of the oldest sedimentary rocks including BIFs and cherts, and have a potential to estimate the Eoarchean surface environments (Fig. 1). Thus, since early 1980s (Appel, 1980), many geochemical studies for the BIFs have been performed for their trace element compositions (Dymek and Klein, 1988; Bolhar et al., 2004), stable isotope ratios of S (Mojzsis et al., 2003; Whitehouse et al., 2005), Si (André et al., 2006) and Fe (Dauphas et al., 2004, 2007; Whitehouse and Fedo, 2007; Yoshiya et al., 2015), Pb isotope systematics (Moorbath et al., 1973; Frei et al., 1999; Frei and Polat, 2007) and Sm–Nd isotope systematics (Shimizu et al., 1990; Frei et al., 1999; Frei and Polat, 2007).

Dymek and Klein (1988) classified the BIFs into quartz–magnetite IF, amphibole-rich magnesian IF, calcite- and dolomite-rich carbonate IF and graphite-, ripidolite- and almandine-rich graphitic and aluminous IF, and analyzed the whole-rock REE compositions. They suggested that they were precipitated from seawater with inputs of high-temperature (>300 °C) hydrothermal fluid because of positive Eu anomalies of the shale-normalized REE + Y patterns. Moreover, they showed that the graphitic and aluminous IFs have higher REE and transition element contents (e.g. Sc, V, Cr, Co, Ni, Cu, Zn, Y, REE and U) than others due to inputs of detrital materials. Bolhar et al. (2004) showed that PAAS-

京都大学 KYOTO UNIVERSITY
A Self-archived copy in
Kyoto University Research Information Repository
https://repository.kulib.kyoto-u.ac.jp
京都大学学術情報リポジトリ KURENAI 紅 Kyoto University Research Information Repository



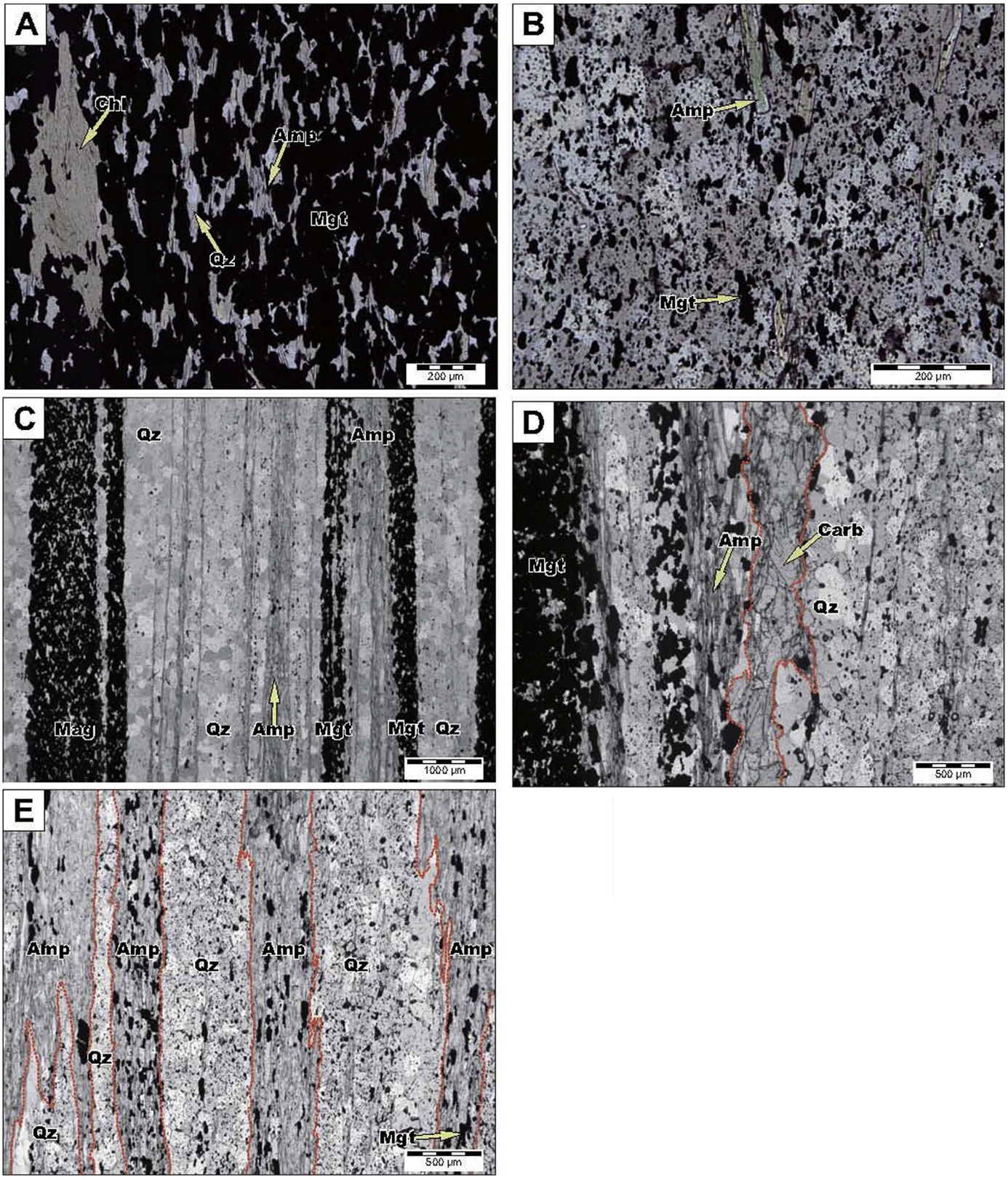


**Figure 4.** Photomicrographs of the BIFs in plane polarized light. (A) A magnified photo of a black layer, which is composed mainly of magnetite, accompanied with quartz, amphibole and chlorite. (B) A gray-colored bands, showing scattered magnetite within quartz matrix. (C) Alternation of black, magnetite-rich bands and white, quartz-rich bands with thin amphibole-rich layers with a nematoblastic texture. (D) Interbedded calcite and amphibole layers interbedded within quartz layer. (E) A magnified photo of a greenish band, which consists of alternating amphibole and quartz with scattered magnetite. Mgt: magnetite, Qz: quartz, Amp: actinolitic amphibole, Chl: ripidolitic chlorite, Hem: hematite and Carb: carbonate mineral (calcite).

京都大学 KYOTO UNIVERSITY
A Self-archived copy in
Kyoto University Research Information Repository
https://repository.kulib.kyoto-u.ac.jp
京都大学学術情報リポジトリ KURENAI 紅 Kyoto University Research Information Repository



**Table 1**
Whole-rock major (in wt.%) and trace element (in ppm) data for the BIFs in the Isua supracrustal belt.

| Sample No. | 9B | 18B | 45B | 54B | 60B | 90B | 138B | 150B | 177B | 193B | 236B | 258B | 277B | 291B | 312B | 7W |
|---|---|---|---|---|---|---|---|---|---|---|---|---|---|---|---|---|
| Type | Black | Black | Black | Black | Black | Black | Black | Black | Black | Black | Black | Black | Black | Black | Black | White |
| Distance[a] (m) | 0.30 | 0.75 | 1.68 | 2.13 | 2.33 | 3.30 | 4.44 | 4.72 | 5.20 | 5.54 | 6.33 | 6.85 | 7.43 | 7.81 | 8.38 | 0.21 |
| $SiO_2$ | 17.2 | 11.4 | 10 | 11.7 | 9.9 | 9.8 | 17.4 | 7.8 | 9.2 | 9.7 | 9.0 | 12.8 | 11.6 | 8.6 | 13.1 | 85.3 |
| $Al_2O_3$ | 0.7 | 0.8 | 0.7 | 0.7 | 1.5 | 0.8 | 0.9 | 1.0 | 0.7 | 0.9 | 0.7 | 0.8 | 0.7 | 0.7 | 0.8 | - |
| $TiO_2$ | 0.10 | 0.11 | 0.12 | 0.12 | 0.11 | 0.11 | 0.12 | 0.12 | 0.10 | 0.12 | 0.11 | 0.12 | 0.12 | 0.12 | 0.11 | - |
| $Fe_2O_3$[b] | 80.4 | 84.7 | 85.5 | 83.8 | 85.4 | 84.8 | 77.2 | 87.4 | 88.0 | 87.3 | 87.9 | 82.5 | 83.8 | 85.6 | 84.4 | 13.6 |
| MgO | 0.68 | 0.107 | 1.65 | 1.86 | 1.56 | 2.37 | 2.34 | 2.00 | 1.01 | 1.00 | 1.17 | 1.74 | 1.86 | 2.20 | 0.74 | 0.42 |
| MnO | 0.1 | 1.5 | 0.12 | 0.12 | 0.12 | 0.12 | 0.12 | 0.12 | 0.12 | 0.11 | 0.11 | 0.12 | 0.12 | 0.13 | 0.10 | 0.02 |
| CaO | 0.67 | 1.36 | 1.66 | 1.59 | 1.26 | 1.93 | 1.85 | 1.59 | 0.87 | 0.90 | 1.04 | 1.80 | 1.67 | 2.29 | 0.74 | 0.29 |
| $Na_2O$ | - | - | - | - | - | - | - | - | - | - | - | - | - | - | - | - |
| $K_2O$ | - | - | - | - | - | - | - | - | - | - | - | - | - | - | - | - |
| $P_2O_5$ | - | - | 0.20 | - | - | 0.11 | 0.08 | - | - | - | - | 0.22 | - | 0.30 | - | - |
| Total | 99.89 | 99.95 | 99.92 | 99.90 | 99.88 | 100.01 | 99.98 | 100.04 | 99.99 | 99.99 | 99.98 | 100.10 | 99.89 | 99.94 | 100.02 | 99.67 |
| Loss of ignition<br>Gain of ignition | 2.06 | 2.47 | 2.63 | 2.41 | 2.47 | 2.44 | 2.38 | 2.30 | 2.34 | 2.84 | 2.73 | 2.39 | 2.29 | 2.51 | 2.55 | 0.16 |
| Li | 0.75 | 0.39 | 0.33 | 0.31 | 0.34 | 1.09 | 1.47 | 1.19 | 0.72 | 1.15 | 0.69 | 0.44 | 0.32 | 0.35 | 0.19 | 0.43 |
| Sc | 0.22 | 0.34 | 0.31 | 0.39 | 0.21 | 0.33 | 0.85 | 0.72 | 0.22 | 0.77 | 0.37 | 0.59 | 0.45 | 0.43 | 0.18 | 0.02 |
| V | 3.43 | 2.39 | 1.98 | 3.01 | 2.29 | 2.31 | 3.76 | 2.10 | 1.71 | 3.73 | 3.33 | 3.23 | 2.34 | 2.00 | 1.97 | 0.16 |
| Co | 2.9 | 4.1 | 4.7 | 4.3 | 4.2 | 1.3 | 4.5 | 4.3 | 5.7 | 4.5 | 4.8 | 2.9 | 3.7 | 4.9 | 3.8 | 0.82 |
| Ni | 24 | 24 | 28 | 26 | 24 | 39 | 94 | 41 | 39 | 52 | 54 | 41 | 25 | 36 | 21 | 5.2 |
| Cu | 2.61 | 2.09 | 0.67 | 1.57 | 0.80 | 0.09 | 0.13 | 0.03 | 0.02 | 0.03 | 1.20 | 0.25 | 0.25 | 0.23 | 0.17 | 0.88 |
| Zn | 12 | 26 | 27 | 25 | 24 | 47 | 63 | 68 | 100 | 60 | 52 | 29 | 25 | 31 | 12 | 6.1 |
| Rb | 0.92 | 0.38 | 0.36 | 0.62 | 0.22 | 3.23 | 2.30 | 1.36 | 2.07 | 1.97 | 1.14 | 0.43 | 0.61 | 0.44 | 0.26 | 0.05 |
| Sr | 0.91 | 1.74 | 4.11 | 2.07 | 2.00 | 3.77 | 8.33 | 6.18 | 3.27 | 6.39 | 4.51 | 4.32 | 2.88 | 6.56 | 1.14 | 0.47 |
| Y | 3.26 | 4.04 | 7.47 | 7.00 | 2.60 | 4.57 | 7.38 | 8.28 | 5.44 | 11.94 | 11.50 | 6.51 | 4.67 | 8.98 | 3.28 | 3.50 |
| Zr | 0.96 | 1.03 | 0.64 | 0.94 | 2.08 | 1.00 | 2.00 | 2.78 | 0.25 | 1.50 | 0.97 | 1.59 | 1.11 | 0.70 | 0.48 | 0.05 |
| Nb | 0.09 | 0.10 | 0.09 | 0.12 | 0.13 | 0.10 | 0.06 | 0.11 | 0.09 | 0.08 | 0.06 | 0.06 | 0.04 | 0.04 | 0.03 | 0.01 |
| Ba | 2.41 | 2.44 | 2.30 | 2.58 | 2.38 | 6.76 | 9.35 | 10.66 | 8.41 | 16.19 | 8.27 | 3.02 | 2.90 | 3.59 | 2.88 | 1.35 |
| La | 3.40 | 2.67 | 1.77 | 3.45 | 1.34 | 4.96 | 10.40 | 1.16 | 0.27 | 5.91 | 3.55 | 8.03 | 3.63 | 9.30 | 1.62 | 0.34 |
| Ce | 4.89 | 3.87 | 2.71 | 5.67 | 1.76 | 6.56 | 13.87 | 1.75 | 0.65 | 8.92 | 4.35 | 10.58 | 4.64 | 9.48 | 2.26 | 0.53 |
| Pr | 0.503 | 0.397 | 0.323 | 0.573 | 0.181 | 0.625 | 1.35 | 0.226 | 0.102 | 0.831 | 0.448 | 1.02 | 0.448 | 0.821 | 0.24 | 0.0743 |
| Nd | 1.72 | 1.38 | 1.40 | 2.13 | 0.688 | 2.07 | 4.30 | 1.06 | 0.57 | 2.69 | 1.69 | 3.38 | 1.48 | 2.6 | 0.91 | 0.407 |
| Sm | 0.207 | 0.228 | 0.342 | 0.363 | 0.134 | 0.293 | 0.559 | 0.330 | 0.176 | 0.430 | 0.358 | 0.406 | 0.180 | 0.357 | 0.163 | 0.155 |
| Eu | 0.147 | 0.198 | 0.311 | 0.272 | 0.119 | 0.243 | 0.359 | 0.279 | 0.174 | 0.338 | 0.336 | 0.228 | 0.121 | 0.254 | 0.117 | 0.153 |
| Gd | 0.230 | 0.311 | 0.537 | 0.476 | 0.208 | 0.381 | 0.622 | 0.530 | 0.311 | 0.646 | 0.603 | 0.418 | 0.242 | 0.505 | 0.189 | 0.286 |
| Tb | 0.0349 | 0.0538 | 0.0910 | 0.0792 | 0.0337 | 0.0537 | 0.0925 | 0.0936 | 0.0511 | 0.1070 | 0.0957 | 0.0603 | 0.0382 | 0.0735 | 0.0301 | 0.0497 |
| Dy | 0.247 | 0.379 | 0.617 | 0.535 | 0.223 | 0.359 | 0.596 | 0.651 | 0.358 | 0.786 | 0.666 | 0.396 | 0.266 | 0.512 | 0.203 | 0.343 |
| Ho | 0.0800 | 0.0964 | 0.1600 | 0.1360 | 0.0588 | 0.0898 | 0.1440 | 0.1630 | 0.0939 | 0.2040 | 0.1770 | 0.1020 | 0.0699 | 0.1340 | 0.0490 | 0.0851 |
| Er | 0.201 | 0.298 | 0.471 | 0.415 | 0.181 | 0.286 | 0.448 | 0.512 | 0.283 | 0.666 | 0.558 | 0.326 | 0.227 | 0.432 | 0.151 | 0.266 |
| Tm | 0.0310 | 0.0460 | 0.0680 | 0.0610 | 0.0280 | 0.0430 | 0.0710 | 0.0730 | 0.0380 | 0.0980 | 0.0760 | 0.0490 | 0.0310 | 0.0620 | 0.0230 | 0.0360 |
| Yb | 0.194 | 0.311 | 0.437 | 0.386 | 0.186 | 0.283 | 0.448 | 0.463 | 0.220 | 0.647 | 0.465 | 0.326 | 0.208 | 0.416 | 0.148 | 0.219 |
| Lu | 0.0368 | 0.0512 | 0.0700 | 0.0633 | 0.0335 | 0.0495 | 0.0738 | 0.0741 | 0.0346 | 0.1090 | 0.0737 | 0.0577 | 0.0343 | 0.0697 | 0.0259 | 0.0359 |
| Hf | 0.0169 | 0.0184 | 0.0129 | 0.0355 | 0.0465 | 0.0233 | 0.0401 | 0.0552 | 0.0048 | 0.0276 | 0.0220 | 0.0291 | 0.0218 | 0.0157 | 0.0070 | 0.0013 |
| Ta | 0.0045 | 0.0033 | 0.0028 | 0.0049 | 0.0051 | 0.0027 | 0.0026 | 0.0047 | 0.0026 | 0.0047 | 0.0031 | 0.0033 | 0.0012 | 0.0014 | 0.0011 | 0.0006 |
| Th | 0.0706 | 0.0200 | 0.0310 | 0.0374 | 0.0435 | 0.0851 | 0.1880 | 0.1250 | 0.0236 | 0.0994 | 0.0385 | 0.0653 | 0.0498 | 0.0398 | 0.0202 | 0.0024 |
| U | 0.0170 | 0.0195 | 0.0128 | 0.0365 | 0.0317 | 0.0125 | 0.0325 | 0.0237 | 0.0110 | 0.0166 | 0.0180 | 0.0062 | 0.0069 | 0.0112 | 0.0064 | 0.0040 |
| Y/Ho | 40.8 | 41.9 | 46.7 | 51.5 | 44.2 | 50.9 | 51.3 | 50.8 | 57.9 | 58.5 | 65.0 | 63.8 | 66.8 | 67.0 | 66.9 | 41.1 |
| $Pr_{PAAS}/Yb_{PAAS}$ | 0.816 | 0.401 | 0.232 | 0.467 | 0.306 | 0.694 | 0.945 | 0.154 | 0.146 | 0.404 | 0.303 | 0.985 | 0.678 | 0.621 | 0.510 | 0.107 |
| La/La* | 1.43 | 1.48 | 1.87 | 1.52 | 1.93 | 1.59 | 1.43 | 2.04 | 1.46 | 1.35 | 2.04 | 1.56 | 1.61 | 2.06 | 1.76 | 2.47 |
| Ce/Ce* | 1.03 | 1.05 | 1.13 | 1.14 | 1.14 | 1.08 | 1.02 | 1.12 | 1.10 | 1.08 | 1.13 | 1.06 | 1.06 | 1.13 | 1.11 | 1.21 |
| Eu/Eu* | 3.36 | 3.58 | 3.54 | 3.19 | 3.56 | 3.80 | 3.06 | 3.19 | 3.68 | 3.16 | 3.64 | 2.79 | 2.90 | 3.11 | 3.28 | 3.48 |

La/La*, Ce/Ce* and Eu/Eu* are defined by $[La/\{Pr/(Pr/Nd)^2\}]_{PAAS}$, $[Ce/\{Pr/(Pr/Nd)\}]_{PAAS}$ and $[Eu/(0.67Sm + 0.33Tb)]_{PAAS}$, respectively.
[a] Distance from the bottom on the greenstones.
[b] Total iron as $Fe_2O_3$.

normalized REE + Y patterns of the BIFs share modern seawater-like character such as positive La ($La_{SN}/(3Pr_{SN} - 2Nd_{SN}) > 1$) and Y (Y/Ho > ca. 26) anomalies and low LREE to HREE ratios ($La_{SN}/Yb_{SN} < 1$) with the exception of Eu ($Eu_{SN}/0.67Sm_{SN} + 0.33Tb_{SN}$) and Ce ($Ce_{SN}/(2Pr_{SN} - Nd_{SN})$) anomalies. However, the relationship of the patterns with lithofacies was still ambiguous due to lack of their mineralogical and major element composition data.

This study presents major and trace element contents of the BIFs systematically collected from stratigraphically lower to upper levels in the ISB to estimate the influences of lithofacies and involvement of clastic and volcanic materials on the whole-rock compositions, and to reconstruct evolutions of transition elements of seawater (e.g. V, Co, Ni and U) through time. Moreover, we estimated the seawater and hydrothermal processes in the Archean oceans, and sedimentary environments of the ISB BIFs based on the relationship between stratigraphy and REE and Y compositions of the BIFs.

## 2. Geological outline and the BIFs descriptions for this study

### 2.1. Geological outline of the Isua supracrustal belt

The 3.8–3.7 Ga Isua supracrustal belt (ISB) is located at approximately 150 km northeast of Nuuk, southern West Greenland. The southern West Greenland is underlain mainly by the Archean orthogneisses, supracrustal rocks and various types of intrusions, and is subdivided into three terranes: Akia, Akulleq and

京都大学 KYOTO UNIVERSITY
A Self-archived copy in
Kyoto University Research Information Repository
https://repository.kulib.kyoto-u.ac.jp
京都大学学術情報リポジトリ KURENAI 紅 Kyoto University Research Information Repository



| 48W | 65W | 216W | 256W | 292W | 168R | 170R | 179R | 26GRY | 61GRY | 89GRY | 187GRY | 236GRY | 260GRY | 303GRY | 11GRN | 60GRN | 259GRN | 268GRN | 327GRN |
|---|---|---|---|---|---|---|---|---|---|---|---|---|---|---|---|---|---|---|---|
| White | White | White | White | White | White | White | White | Gray | Gray | Gray | Gray | Gray | Gray | Gray | Green | Green | Green | Green | Green |
| 1.82 | 2.50 | 5.85 | 6.79 | 7.85 | 5.08 | 5.13 | 5.32 | 1.11 | 2.41 | 3.25 | 5.46 | 6.29 | 6.93 | 8.15 | 0.39 | 2.37 | 6.88 | 7.17 | 8.78 |
| 97.9 | 86.8 | 89.2 | 92.2 | 95.6 | 74.3 | 79.2 | 63.3 | 89.2 | 88.7 | 85.9 | 81.4 | 53.2 | 63.6 | 88.5 | 64.8 | 37.0 | 45.7 | 82.2 | 62.6 |
| - | - | - | - | - | - | - | - | - | - | - | - | - | - | - | - | 0.7 | - | - | - |
| - | - | - | - | - | - | - | - | - | - | - | - | - | - | - | - | - | - | - | - |
| 1.45 | 11.3 | 9.97 | 5.40 | 3.95 | 24.3 | 19.2 | 34.3 | 10.4 | 10.5 | 11.8 | 17.7 | 42.2 | 32.7 | 10.7 | 31.3 | 52.3 | 47.3 | 12.9 | 23.9 |
| 0.10 | 1.05 | 0.32 | 1.12 | 0.11 | 0.56 | 0.42 | 0.90 | 0.09 | 0.25 | 1.21 | 0.07 | 2.21 | 1.76 | 0.36 | 1.07 | 5.44 | 3.71 | 2.42 | 6.81 |
| 0.01 | 0.04 | 0.02 | 0.03 | 0.02 | 0.04 | 0.03 | 0.05 | 0.02 | 0.02 | 0.02 | 0.02 | 0.08 | 0.06 | 0.02 | 0.03 | 0.12 | 0.12 | 0.05 | 0.12 |
| 0.15 | 0.65 | 0.32 | 0.93 | 0.15 | 0.56 | 0.38 | 1.19 | 0.11 | 0.21 | 0.89 | 0.17 | 1.90 | 1.57 | 0.34 | 2.24 | 4.42 | 2.60 | 1.99 | 5.88 |
| - | - | - | - | - | - | - | - | - | - | - | - | - | - | - | - | - | - | - | - |
| - | - | - | - | - | - | - | - | - | - | - | - | - | - | - | - | - | - | - | - |
| - | - | - | - | - | - | - | - | - | - | - | - | 0.08 | - | - | - | - | - | - | 0.29 |
| 99.61 | 99.81 | 99.83 | 99.68 | 99.83 | 99.77 | 99.21 | 99.73 | 99.79 | 99.67 | 99.85 | 99.39 | 99.67 | 99.64 | 99.87 | 99.41 | 99.93 | 99.44 | 99.58 | 99.56 |
| 0.29 | 0.02 | | 0.08 | 0.08 | | | | 0.05 | | | | | | | 0.29 | | | 0.12 | |
| | | 0.14 | | | 0.31 | 0.46 | 0.52 | | 0.16 | 0.13 | 0.45 | 1.02 | 0.71 | 0.16 | | 1.08 | 1.05 | | 0.09 |
| 0.49 | 0.43 | 0.73 | 0.54 | 0.59 | 0.57 | 0.67 | 0.71 | 0.37 | 0.30 | 0.36 | 0.67 | 0.64 | 0.60 | 0.35 | 0.73 | 0.87 | 0.57 | 0.50 | 0.63 |
| 0.02 | 0.08 | 0.04 | 0.04 | 0.01 | 0.05 | 0.05 | 0.13 | 0.04 | 0.04 | 0.07 | 0.02 | 0.14 | 0.02 | 0.05 | 0.55 | 1.10 | 0.29 | 0.16 | 0.65 |
| 0.04 | 0.430 | 0.07 | 0.04 | 0.07 | 0.19 | 0.29 | 0.37 | 0.18 | 0.34 | 0.23 | 0.29 | 0.82 | 0.11 | 0.20 | 0.56 | 0.45 | 0.77 | 0.44 | 0.32 |
| 0.30 | 0.61 | 0.30 | 0.35 | 0.51 | 0.79 | 1.1 | 1.4 | 1.5 | 0.66 | 0.27 | 1.0 | 1.7 | 0.78 | 0.87 | 6.9 | 4.9 | 3.1 | 2.5 | 6.1 |
| 1.9 | 4.0 | 1.4 | 1.8 | 3.5 | 4.7 | 6.0 | 7.0 | 11 | 3.3 | 7.9 | 7.0 | 18 | 3.4 | 3.2 | 41 | 38 | 20 | 13 | 51 |
| 2.40 | 2.77 | 1.16 | 0.90 | 0.69 | 0.23 | 0.31 | 0.34 | 2.55 | 1.07 | 2.35 | 0.20 | 1.51 | 0.71 | 0.57 | 4.67 | 2.89 | 1.17 | 11.70 | 4.32 |
| 5.3 | 6.1 | 5.1 | 13 | 9.0 | 19.9 | 26.5 | 29.5 | 17 | 4.9 | 14 | 31 | 39 | 13 | 8.8 | 110 | 110 | 48 | 57 | 80 |
| 0.02 | 0.06 | 0.06 | 0.06 | 0.04 | 0.20 | 0.21 | 0.33 | 0.06 | 0.04 | 0.08 | 0.38 | 0.24 | 0.09 | 0.07 | 0.12 | 0.15 | 0.20 | 0.16 | 0.27 |
| 0.68 | 0.95 | 1.95 | 1.44 | 0.55 | 6.10 | 3.96 | 23.41 | 0.50 | 0.58 | 1.13 | 2.56 | 3.08 | 0.76 | 0.67 | 4.78 | 5.26 | 3.98 | 2.25 | 8.28 |
| 1.54 | 1.14 | 1.44 | 4.69 | 2.01 | 3.53 | 3.88 | 6.28 | 8.87 | 1.17 | 1.51 | 4.13 | 8.90 | 2.57 | 4.43 | 38.70 | 24.60 | 7.09 | 10.60 | 19.10 |
| 0.09 | 0.21 | 0.14 | 0.06 | 0.05 | 0.10 | 0.12 | 0.29 | 0.06 | 0.13 | 0.11 | 0.08 | 0.18 | 0.05 | 0.08 | 0.48 | 0.77 | 0.38 | 0.23 | 0.27 |
| 0.00 | 0.02 | 0.00 | 0.00 | 0.00 | 0.02 | 0.02 | 0.03 | 0.01 | 0.01 | 0.02 | 0.01 | 0.02 | 0.00 | 0.00 | 0.11 | 0.08 | 0.09 | 0.02 | 0.02 |
| 1.06 | 3.28 | 3.11 | 1.27 | 3.38 | 11.09 | 15.47 | 16.11 | 2.13 | 1.25 | 1.46 | 13.5 | 3.92 | 4.17 | 1.03 | 6.50 | 3.11 | 15.40 | 3.99 | 1.27 |
| 0.54 | 0.14 | 0.78 | 0.81 | 0.32 | 0.29 | 0.53 | 0.48 | 0.61 | 0.35 | 0.09 | 0.35 | 2.98 | 0.27 | 0.34 | 2.58 | 0.31 | 0.94 | 0.79 | 5.69 |
| 0.69 | 0.23 | 0.87 | 1.14 | 0.37 | 0.54 | 0.80 | 0.84 | 1.17 | 0.51 | 0.16 | 0.57 | 3.79 | 0.48 | 0.54 | 4.95 | 1.00 | 1.52 | 1.33 | 11.36 |
| 0.0715 | 0.024 | 0.0831 | 0.119 | 0.06 | 0.07 | 0.103 | 0.12 | 0.178 | 0.056 | 0.0241 | 0.0831 | 0.396 | 0.0543 | 0.0696 | 0.739 | 0.212 | 0.184 | 0.151 | 0.907 |
| 0.274 | 0.11 | 0.324 | 0.51 | 0.254 | 0.344 | 0.474 | 0.616 | 0.949 | 0.216 | 0.138 | 0.404 | 1.52 | 0.282 | 0.338 | 4.04 | 1.52 | 0.86 | 0.744 | 3.72 |
| 0.054 | 0.037 | 0.068 | 0.133 | 0.060 | 0.092 | 0.111 | 0.167 | 0.336 | 0.050 | 0.047 | 0.103 | 0.313 | 0.092 | 0.108 | 1.314 | 0.811 | 0.272 | 0.262 | 0.831 |
| 0.0598 | 0.0340 | 0.0580 | 0.131 | 0.0478 | 0.0838 | 0.107 | 0.146 | 0.331 | 0.0465 | 0.0544 | 0.0952 | 0.2970 | 0.0856 | 0.0990 | 1.38 | 0.793 | 0.240 | 0.255 | 0.636 |
| 0.099 | 0.064 | 0.098 | 0.250 | 0.108 | 0.164 | 0.198 | 0.313 | 0.604 | 0.078 | 0.089 | 0.202 | 0.552 | 0.167 | 0.193 | 2.427 | 1.516 | 0.355 | 0.530 | 1.310 |
| 0.0178 | 0.0115 | 0.0157 | 0.0416 | 0.0170 | 0.0268 | 0.0305 | 0.0546 | 0.1200 | 0.0141 | 0.0161 | 0.0328 | 0.0862 | 0.0294 | 0.0393 | 0.4070 | 0.2960 | 0.0598 | 0.1050 | 0.2070 |
| 0.138 | 0.083 | 0.106 | 0.303 | 0.119 | 0.193 | 0.220 | 0.409 | 0.905 | 0.099 | 0.121 | 0.242 | 0.602 | 0.208 | 0.299 | 2.963 | 2.262 | 0.425 | 0.816 | 1.408 |
| 0.0378 | 0.0212 | 0.0269 | 0.0803 | 0.0324 | 0.0525 | 0.0586 | 0.1060 | 0.2370 | 0.0250 | 0.0320 | 0.0700 | 0.1510 | 0.0550 | 0.0760 | 0.7800 | 0.5900 | 0.1140 | 0.2180 | 0.3480 |
| 0.128 | 0.069 | 0.081 | 0.243 | 0.103 | 0.164 | 0.189 | 0.342 | 0.780 | 0.078 | 0.103 | 0.208 | 0.476 | 0.171 | 0.257 | 2.470 | 1.923 | 0.362 | 0.715 | 1.059 |
| 0.0190 | 0.0100 | 0.0110 | 0.0340 | 0.0150 | 0.0220 | 0.0260 | 0.0500 | 0.1200 | 0.0120 | 0.0150 | 0.0280 | 0.0620 | 0.0250 | 0.0400 | 0.3500 | 0.3000 | 0.0560 | 0.1000 | 0.1500 |
| 0.118 | 0.0746 | 0.0664 | 0.210 | 0.101 | 0.141 | 0.160 | 0.328 | 0.747 | 0.0764 | 0.104 | 0.175 | 0.365 | 0.155 | 0.270 | 2.18 | 2.12 | 0.392 | 0.648 | 0.969 |
| 0.0187 | 0.0122 | 0.0099 | 0.0333 | 0.0185 | 0.0231 | 0.0281 | 0.0502 | 0.1210 | 0.0122 | 0.0162 | 0.0292 | 0.0615 | 0.0255 | 0.0458 | 0.3640 | 0.3270 | 0.0679 | 0.1080 | 0.1600 |
| 0.0012 | 0.0042 | 0.0031 | 0.0018 | 0.0012 | 0.0026 | 0.0030 | 0.0068 | 0.0022 | 0.0033 | 0.0027 | 0.0018 | 0.0036 | 0.0007 | 0.0013 | 0.0222 | 0.0360 | 0.0144 | 0.0074 | 0.0127 |
| 0.0002 | 0.0009 | 0.0002 | 0.0003 | 0.0001 | 0.0007 | 0.0008 | 0.0012 | 0.0007 | 0.0007 | 0.0005 | 0.0006 | 0.0006 | 0.0002 | 0.0002 | 0.0056 | 0.0024 | 0.0022 | 0.0014 | 0.0026 |
| 0.0031 | 0.0131 | 0.0044 | 0.0030 | 0.0084 | 0.0038 | 0.0045 | 0.0091 | 0.0048 | 0.0106 | 0.0089 | 0.0063 | 0.0143 | 0.0047 | 0.0040 | 0.0252 | 0.0204 | 0.0567 | 0.0364 | 0.0370 |
| 0.0147 | 0.0079 | 0.0027 | 0.0056 | 0.0092 | 0.0095 | 0.0078 | 0.0091 | 0.0196 | 0.0082 | 0.0034 | 0.0060 | 0.0136 | 0.0206 | 0.0045 | 0.0586 | 0.0215 | 0.0125 | 0.0182 | 0.0659 |
| 40.7 | 53.8 | 53.5 | 58.4 | 62.0 | 67.2 | 66.2 | 59.2 | 37.4 | 46.6 | 47.3 | 59.0 | 58.9 | 47.1 | 58.3 | 49.6 | 41.7 | 62.2 | 48.6 | 54.9 |
| 0.191 | 0.101 | 0.394 | 0.178 | 0.187 | 0.156 | 0.202 | 0.115 | 0.0750 | 0.231 | 0.0729 | 0.149 | 0.342 | 0.110 | 0.0811 | 0.107 | 0.0314 | 0.147 | 0.0733 | 0.294 |
| 1.99 | 2.25 | 2.60 | 2.25 | 1.73 | 1.80 | 1.98 | 1.94 | 1.75 | 1.67 | 2.15 | 1.79 | 1.99 | 2.45 | 2.10 | 1.89 | 1.37 | 2.04 | 2.29 | 1.91 |
| 1.15 | 1.37 | 1.27 | 1.27 | 0.80 | 1.17 | 1.12 | 1.12 | 1.09 | 1.08 | 1.18 | 1.03 | 1.13 | 1.42 | 1.16 | 1.13 | 1.06 | 1.20 | 1.34 | 1.59 |
| 3.87 | 3.28 | 3.55 | 3.52 | 3.00 | 3.38 | 3.69 | 3.06 | 3.28 | 3.53 | 3.95 | 3.28 | 3.62 | 3.30 | 3.03 | 3.78 | 3.22 | 3.76 | 3.03 | 3.07 |

Tasiusarsuaq terranes from north to south (Fig. 1A). The Akulleq terrane is composed mainly of the Eoarchean Itsaq gneisses (3830–3660 Ma) and old supracrustal rocks (Akilia association), the Paleoarchean mafic intrusions (Ameralik dykes) and the Neoarchean Ikkattoq gneisses (2820 Ma) and young supracrustal rocks (Malene supracrustals) (Friend et al., 1988; McGregor et al., 1991; McGregor, 1993).

The ISB is the largest belt of the Akilia association and forms a 35 km long arcuate tract in the northern end of the Akulleq terrane (Fig. 1A). The ISB comprises 3.8–3.7 Ga volcanic and sedimentary rocks (Nutman et al., 1993, 1996; Crowley et al., 2002; Crowley, 2003; Nutman et al., 2007; Nutman and Friend, 2009), and it is considered that it occurs as an enclave within the Itsaq Gneiss (Fig. 1B). The ISB is composed mainly of four lithofacies (Komiya et al., 1999): (1) mafic-felsic clastic sedimentary rocks including black shale and minor conglomerate, (2) chemical sedimentary rocks of BIFs, chert and carbonate rocks, (3) basaltic and basaltic andesitic volcanic rocks including pillow lava, pillow breccia, and related intrusive rocks and (4) ultramafic rocks. They were subsequently intruded by the Paleoarchean Ameralik (Tarssartoq) dykes, and the Proterozoic N–S-trending high-Mg andesite dikes (Nutman, 1986).

Although it was previously considered that the ISB comprises volcano-sedimentary successions, it has, recently, been widely considered that it is composed of some tectonic slices bounded by faults (Nutman, 1986; Appel et al., 1998; Komiya et al., 1999; Myers, 2001; Rollinson, 2002, 2003; Nutman and Friend, 2009). But, the origins of the tectonic slices are controversial, and two ideas were

京都大学 KYOTO UNIVERSITY
A Self-archived copy in
Kyoto University Research Information Repository
https://repository.kulib.kyoto-u.ac.jp
京都大学学術情報リポジトリ KURENAI 紅 Kyoto University Research Information Repository



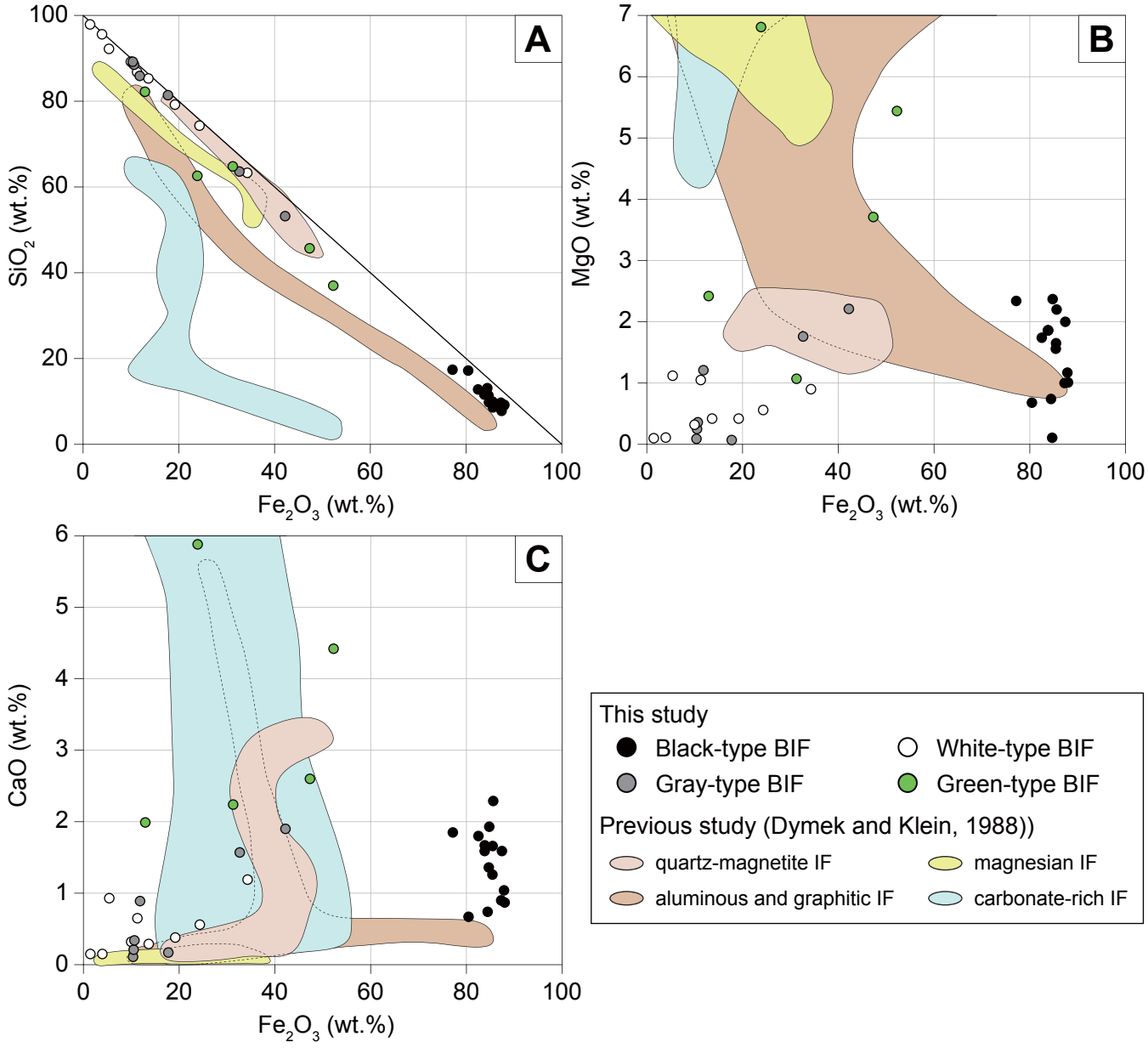


**Figure 5.** $Fe_2O_3$ variation diagrams for (A) $SiO_2$, (B) MgO, (C) CaO contents along with compositional variations of BIFs from a literature (Dymek and Klein, 1988).

mainly proposed: collision and amalgamation of allochthonous terranes and peeling and accretion of oceanic crusts during successive accretion of oceanic crusts, respectively (e.g. Komiya et al., 1999; Nutman and Friend, 2009). The former is that the slices or panels were formed after the intrusions of the granitic rocks, due to collision and amalgamation of some terranes with different geologic histories (e.g. Nutman, 1986; Nutman et al., 1997a; Rollinson, 2002, 2003; Crowley, 2003; Nutman and Friend, 2009). Especially, Nutman and the colleagues proposed that the ISB comprises two tectonic belts with different origins based on age distributions of detrital zircons in quartzite and felsic sedimentary rocks and orthogneisses intruding into the supracrustal belts (Nutman et al., 1997a; Crowley, 2003; Nutman and Friend, 2009; Nutman et al., 2009). The latter is that the tectonic slices are bounded by layer-parallel faults and were formed during accretion of oceanic materials to a continental crust (Komiya et al., 1999).

The tectonic setting of the ISB is still controversial. Furnes and the colleagues showed an ophiolite-like stratigraphy including pillow lavas and sheeted dykes and estimated that they were formed in the intra-oceanic island arc or mid-oceanic ridge settings based on the geological occurrence and geochemistry of the greenstones (Furnes et al., 2007, 2009). On the other hand, some groups suggested that the ISB was formed in a subduction zone environment because the greenstones share geochemical signatures with the modern boninites and island arc basalts (Polat et al., 2002; Polat and Hofmann, 2003; Polat and Frei, 2005; Dilek and Polat, 2008; Polat et al., 2015). In the case, the BIFs were formed in spreading fore-arc and intra-arc settings associated with trench

京都大学 KYOTO UNIVERSITY
A Self-archived copy in
Kyoto University Research Information Repository
https://repository.kulib.kyoto-u.ac.jp
京都大学学術情報リポジトリ KURENAI 紅 Kyoto University Research Information Repository



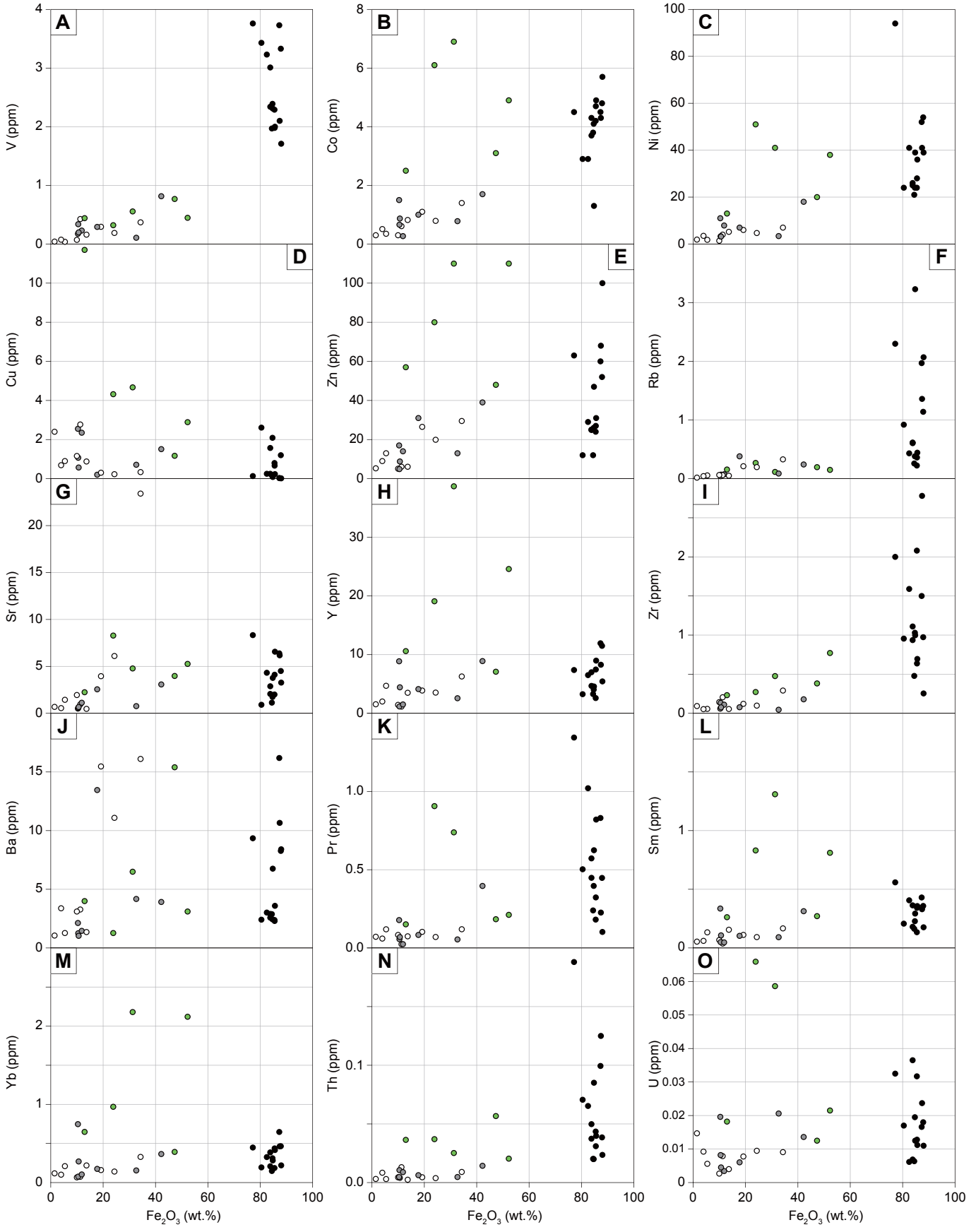


**Figure 6.** $Fe_2O_3$ variation diagrams for (A) V, (B) Co, (C) Ni, (D) Cu, (E) Zn, (F) Rb, (G) Sr, (H) Y, (I) Zr, (J) Ba, (K) Pr, (L) Sm, (M) Yb, (N) Th and (O) U contents. The symbols are same as those in Fig. 5.

京都大学 KYOTO UNIVERSITY
A Self-archived copy in
Kyoto University Research Information Repository
https://repository.kulib.kyoto-u.ac.jp
京都大学学術情報リポジトリ KURENAI 紅 Kyoto University Research Information Repository



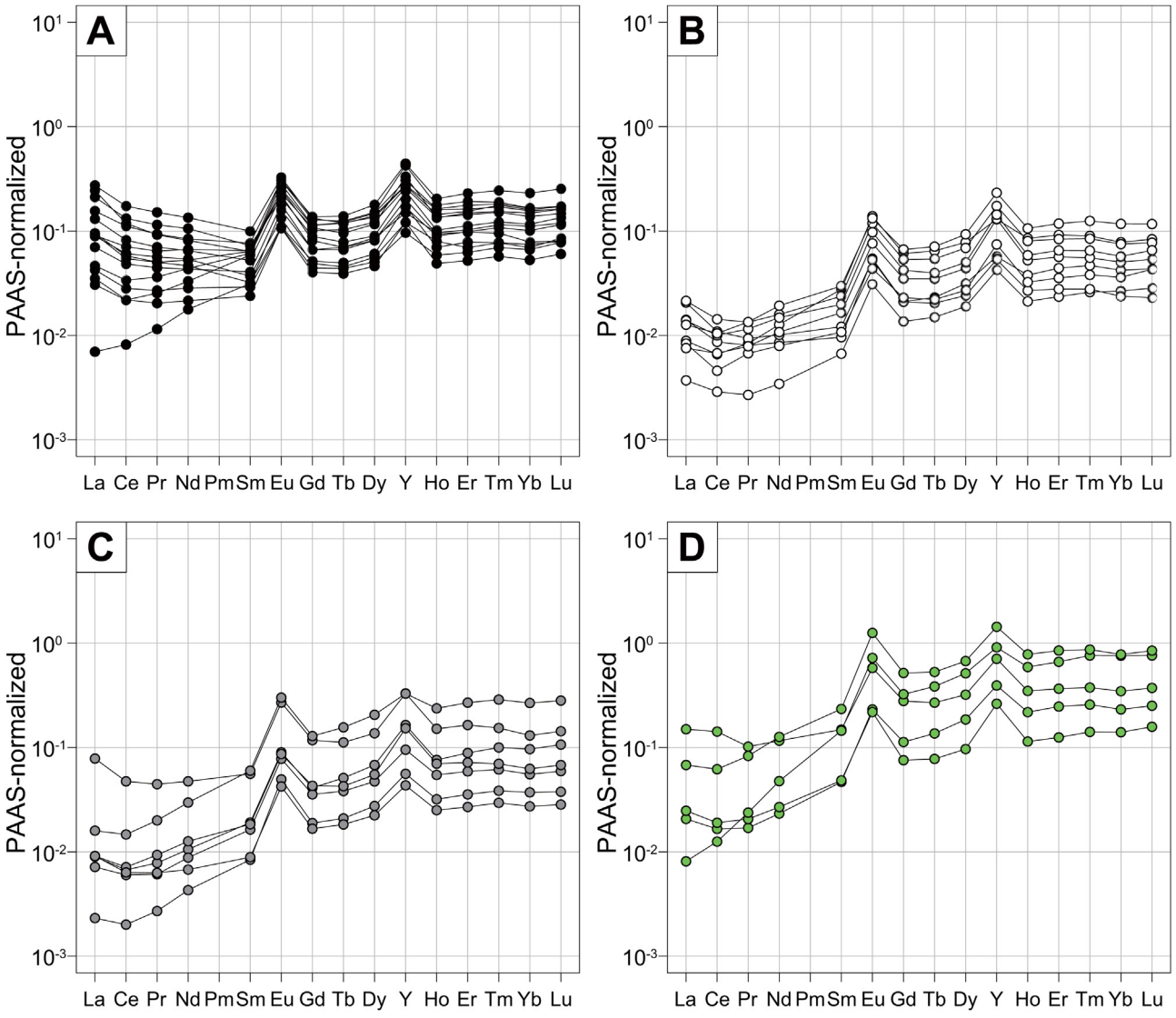


**Figure 7.** PAAS-normalized REE + Y patterns for (A) Black-type, (B) White-type, (C) Gray-type and (D) Green-type BIFs.

rollback caused by young and hot oceanic crust (Polat and Frei, 2005; Dilek and Polat, 2008; Polat et al., 2015). Komiya and colleagues proposed that the depositional environment ranged from basaltic volcanism at a mid-oceanic ridge through deposition of deep-sea sediments (BIFs/chert) in an open sea to terrigenous sedimentation at the subduction zone based on the OPS-like stratigraphy (Komiya et al., 1999, 2015; Yoshiya et al., 2015).

The ISB suffered polyphase metamorphism from greenschist to amphibolite facies (Nutman et al., 1984; Nutman, 1986; Rose et al., 1996; Rosing et al., 1996; Hayashi et al., 2000; Myers, 2001; Komiya et al., 2002; Rollinson, 2002, 2003; Arai et al., 2015). Although it is still controversial whether the variation of mineral parageneses and compositions is due to progressive or retrogressive metamorphism (Nutman, 1986), the variation of mineral parageneses and compositions of mafic and pelitic rocks in the northeastern area of the ISB suggested the progressive metamorphic zonation from greenschist (Zone A) through albite–epidote–amphibolite (Zone B) to amphibolite facies (Zones C and D). The metamorphic pressures and temperatures were estimated 5–7 kbar and 380–550 °C in Zones B to D by garnet–hornblende–plagioclase–quartz and garnet–biotite geothermobarometries (Hayashi et al., 2000; Komiya et al., 2002; Arai et al., 2015).

### 2.2. Geological characteristics of the BIFs

The BIFs and cherts occur as some layers throughout the ISB (Allaart, 1976; Nutman, 1986; Nutman et al., 1996; Nutman et al., 1997b, 2002; Komiya et al., 1999; Nutman and Friend, 2009). We studied the BIFs in the northeastern part of the ISB, corresponding to the metamorphic Zone A (Hayashi et al., 2000) (Figs. 1B and 2A). In this area, the supracrustal rocks have NE-trending strikes with E-dipping, and the stratigraphy of supracrustal rocks in each subunit is composed of pillow lava or massive lava greenstones overlain by BIFs and cherts. The BIFs, ca. 9 m thick, show mappable-scale syncline structures with underlying pillow lava and hyaloclastite-like greenstones (Fig. 2A–C). We collected the BIF samples from the bottom on the hyaloclastite-like greenstones to the top in one-side limb of the syncline structures.

### 2.3. Lithological characteristics of the BIFs for this study

The studied BIFs have sharply-bounded bands with several to tens millimeter thickness. The bands are varied in color even within an outcrop: black, white, gray and green in color, dependent on mineral assemblages but independent of their stratigraphy (Fig. 3).

京都大学 KYOTO UNIVERSITY
A Self-archived copy in
Kyoto University Research Information Repository
https://repository.kulib.kyoto-u.ac.jp
京都大学学術情報リポジトリ KURENAI 紅 Kyoto University Research Information Repository



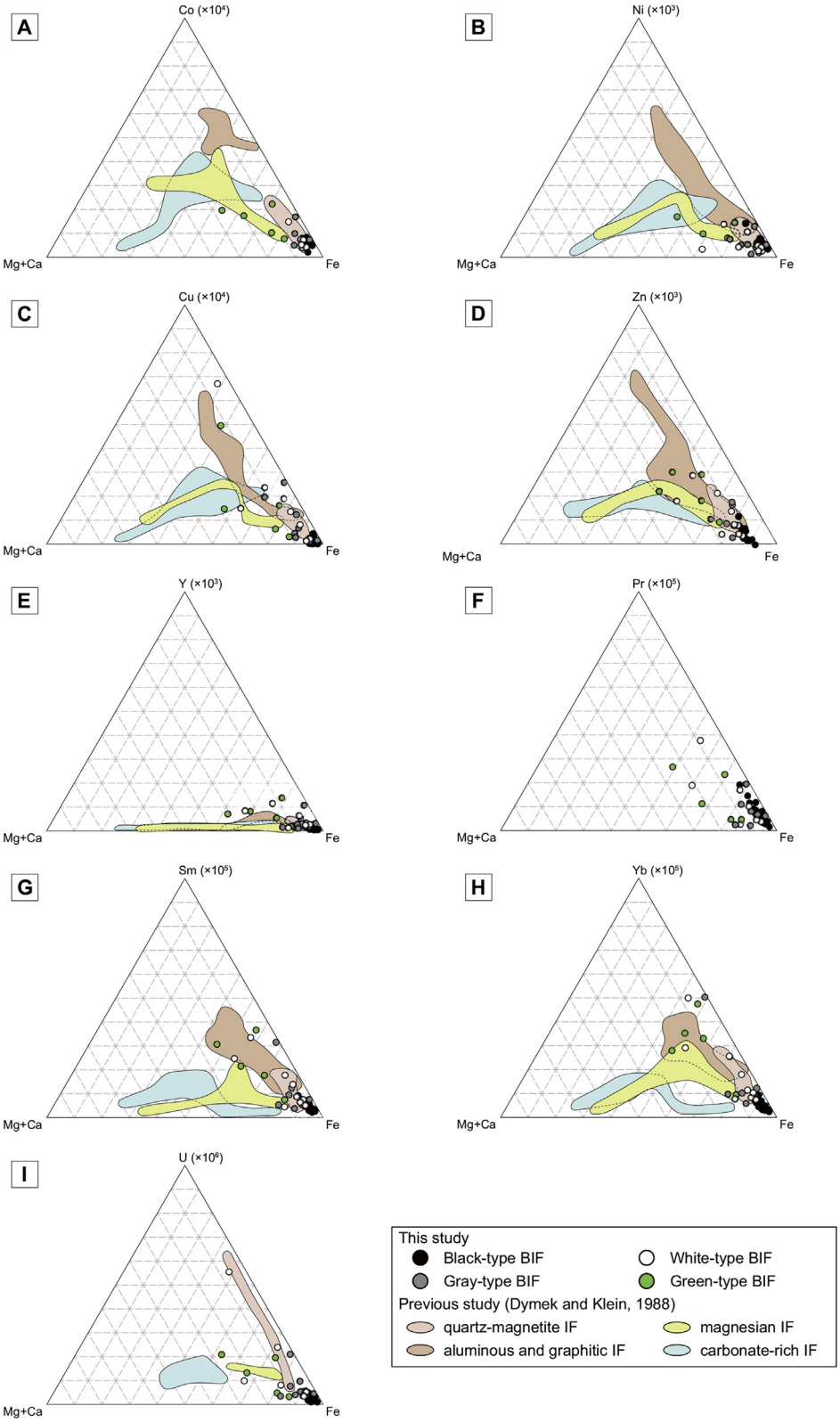


**Figure 8.** Ternary plots of (A) Co–(Mg + Ca)–Fe, (B) Ni–(Mg + Ca)–Fe, (C) Cu–(Mg + Ca)–Fe, (D) Zn–(Mg + Ca)–Fe, (E) Y–(Mg + Ca)–Fe, (F) Pr–(Mg + Ca)–Fe, (G) Sm–(Mg + Ca)–Fe, (H) Yb–(Mg + Ca)–Fe, and (I) U–(Mg + Ca)–Fe contents, along with compositional variations of BIFs from a literature except for Pr (Dymek and Klein, 1988).

京都大学 KYOTO UNIVERSITY
A Self-archived copy in
Kyoto University Research Information Repository
https://repository.kulib.kyoto-u.ac.jp
京都大学学術情報リポジトリ KURENAI 紅 Kyoto University Research Information Repository



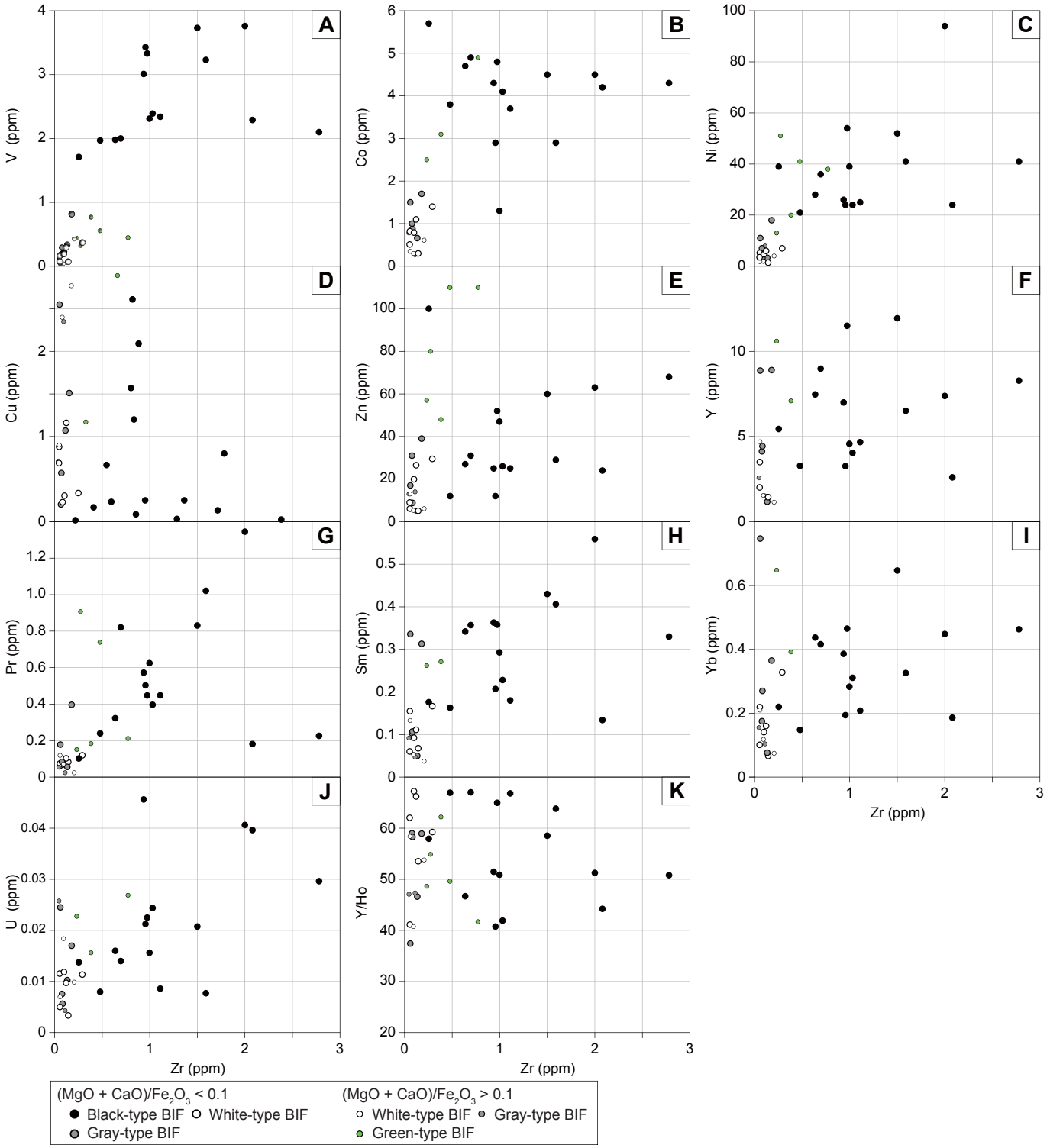


**Figure 9.** Zr variation diagrams of (A) V, (B) Co, (C) Ni, (D) Cu, (E) Zn, (F) Y, (G) Pr, (H) Sm, (I) Yb, (J) U and (K) Y/Ho ratio. Small circles mean samples with high (MgO + CaO)/$Fe_2O_3$ ratios (>0.1).

京都大学 KYOTO UNIVERSITY
A Self-archived copy in
Kyoto University Research Information Repository
https://repository.kulib.kyoto-u.ac.jp
京都大学学術情報リポジトリ KURENAI 紅 Kyoto University Research Information Repository



Mineral assemblages of the BIFs are composed mainly of magnetite + quartz + amphibole (Fig. 4), which are typical mineral assemblage of the moderately metamorphosed BIFs (Klein, 2005), but the modal abundances of the constituent minerals are varied so that their colors are variable.

The black bands are composed mainly of euhedral and anhedral magnetite. They are elongated in the direction parallel to their banding structure. Quartz, actinolitic amphiboles and ripidolitic chlorites are scattered among magnetites (Fig. 4A).

The white and gray bands are composed mainly of quartz, most of which show sutured grains boundary or wavy extinction suggestive of secondary deformation. Magnetites, amphiboles and subordinate amount of calcites ubiquitously occur among the quartz grains or as inclusions within the quartz grains (Fig. 4B). The gray-colored bands are enriched in magnetite as inclusions within quartz matrix relative to the white bands (Fig. 4B). Moreover, most of the bands are interbedded with thin nematoblastic amphibole (Fig. 4C), calcite (Fig. 4D) and magnetite layers.

The green bands consist mainly of alternating actinolite- and quartz-rich layers (Fig. 4E), and the amphiboles show a nematoblastic texture, forming the bands. Anhedral magnetites are scattered as inclusions within the amphibole and quartz. Calcites rarely occur as inclusions within amphiboles.

## 3. Analytical methods

We collected the BIFs from the bottom to the top of the BIF succession (Fig. 2C), and analyzed whole rock compositions of major and trace elements with major focus on REE and other transition elements. The rocks samples were slabbed with a diamond-bladed rock saw to avoid visible altered parts and veins of quartz. Each rock piece consists of some mesobands with different colors, but was classified into four groups based on the colors of dominant bands: Black-, White-, Gray- and Green-types, respectively. They were polished with a grinder for removing saw marks, and rinsed in an ultrasonic bath. They were crushed into small pieces with a hammer wrapped with plastic bags, and ground into powders by an agate mortar.

Major element compositions of the 36 samples were determined with an X-ray fluorescence spectrometry, RIGAKU 3270 (Rigaku Corp., Japan) at the Ocean Research Institute, the University of Tokyo. The analytical reproducibilities are better than 1.0% for $SiO_2$, $TiO_2$, $Al_2O_3$, $Fe_2O_3$, MgO, CaO and $K_2O$, 1.2% for $P_2O_5$, 1.4% for MnO, and 1.6% for $Na_2O$, respectively. The details of XRF analytical procedure were described elsewhere (Kato et al., 1998).

Trace element compositions were determined by a Q-pole mass filter ICP mass spectrometer, iCAP Qc (Thermo Fisher Scientific Inc., USA) with a collision cell at the Kyoto University. The same rock powders as those for major-element analysis were completely digested with 1 mL HF and 1 mL $HClO_4$ in a tightly sealed 7 mL Teflon PFA screw-cap beaker, heated at 120 °C during 12 h with several sonication steps, and then evaporated at 120 °C for 12 h, 165 °C for 12 h and 195 °C for complete dry. The residues were repeatedly digested with 1 mL $HClO_4$ for removing fluoride, completely evaporated again, dissolved with 1 mL HCl and evaporated at 100 °C. The dried residues were digested and diluted in mixtures of 0.5 M $HNO_3$ and trace HF. Before analyses, indium and bismuth solutions were added for internal standards. As the external calibration standard, W-2, issued by USGS, was analyzed every two unknown samples. The preferred values of W-2 by Eggins et al. (1997), except for Tm (Dulski, 2001) were adopted. On the ICP-MS analysis, He + $H_2$ collision gas was introduced in order to eliminate molecular interferences, resulting in low oxide formation ($CeO^+/Ce^+ < \sim 0.5\%$). The reproducibility and accuracies of the analytical protocol were verified with a USGS standard of BIR-1. The reproducibilities (RSD) were under than 5% (2sd) except for Li and Th (Supplementary Table 1). The REE and Y concentrations were normalized by PAAS (Post-Archean Australian Shale, Taylor and McLennan, 1985), and La, Ce and Eu anomalies, La/La*, Ce/Ce* and Eu/Eu*, were defined by $[La_{SN}/\{Pr_{SN}/(Pr_{SN}/Nd_{SN})^2\}]$, $[Ce_{SN}/\{Pr_{SN}/(Pr_{SN}/Nd_{SN})\}]$ and $[Eu_{SN}/(0.67Sm_{SN}+0.33Tb_{SN})]$.

## 4. Result

### 4.1. Major element abundances

Major element compositions of all analyzed samples are listed in Table 1. The BIFs are composed mainly of $Fe_2O_3$ and $SiO_2$ (Fig. 5A), similar to compositions of quartz–magnetite IFs (Dymek and Klein, 1988). The Black-type is enriched in $Fe_2O_3$ whereas the White-type in $SiO_2$ contents. The Gray- and Green-types have the intermediate compositions between the Black- and White-types on the $Fe_2O_3$ vs. $SiO_2$ diagram. The Green-type is off the $SiO_2$–$Fe_2O_3$ line because they contain more abundant other elements such as MgO (1–7 wt.%) and CaO contents (2–6 wt.%) (Fig. 5) so that they are similar to magnesian and carbonate IF (Dymek and Klein, 1988). All the types apparently lack $Na_2O$ and $K_2O$ contents, but contain trace amounts of $P_2O_5$. Most samples except for 60B and 150B have quite low $Al_2O_3$ contents, <1 wt.%.

### 4.2. Trace element abundances

Trace element compositions are also listed in Table 1. $Fe_2O_3$ variation diagrams of Y, Pr, Sm, Yb, Sc, V, Co, Ni, Cu, Zn, Rb, Sr, Ba, Zr, Hf, Th and U contents are shown in Fig. 6. Although the Black-type BIFs have large variations in the trace element contents, they have higher maximum values than other types, except for some elements of the Green-type. The Green-type BIFs are enriched in most REEs, transition elements of Co, Ni, Cu, Zn and U, and high field strength elements (HFSEs) of Zr, Hf and Th. The element contents of the White-, Gray- and Black-types increase with increasing iron contents except for Sr and Ba (Fig. 6). Some White- and Gray-types are extremely enriched in Sr (e.g. 179R) and Ba (e.g. 168R, 170R, 179R and 26GRY) relative to other samples (Fig. 6).

The PAAS-normalized REE + Y patterns of the Black-, White-, Gray- and Green-types are shown in Fig. 7. All of them share some geochemical features: positive La anomalies ($La/La^* > 1$), positive Eu anomalies ($Eu/Eu^* > 1$), positive Y anomalies ($Y/Ho > 26$), and lack to slightly positive Ce anomalies ($1 < Ce/Ce^* < 1.5$) except for one sample (292W). Most of the Black-type BIFs except for three samples of 45B, 150B and 177B ($0.15 < Pr_{SN}/Yb_{SN} < 0.23$) display flat to slightly LREE-enriched REE + Y patterns ($0.30 < Pr_{SN}/Yb_{SN} < 0.99$) whereas the White- and Gray-type BIFs show flat to LREE-depleted REE + Y patterns ($0.07 < Pr_{SN}/Yb_{SN} < 0.39$) (Fig. 7). The REE + Y patterns of the Green-type is highly variable, and different from others in some characteristics. Most of them have much higher REE contents than others, and strongly HREE-enriched REE + Y patterns ($0.03 < Pr_{SN}/Yb_{SN} < 0.29$) (Fig. 7D).

## 5. Discussion

### 5.1. The relationships between the whole-rock trace element contents and lithofacies

The BIFs consist mainly of quartz and iron oxide minerals of hematite and magnetite. Because the quartz-rich BIFs and cherts have lower REE and transition metal contents, amounts of quartz apparently dilute their contents. And, the precursors of the iron-oxide minerals probably hosted the elements because the REE

京都大学 KYOTO UNIVERSITY
A Self-archived copy in
Kyoto University Research Information Repository
https://repository.kulib.kyoto-u.ac.jp
京都大学学術情報リポジトリ KURENAI 紅 Kyoto University Research Information Repository



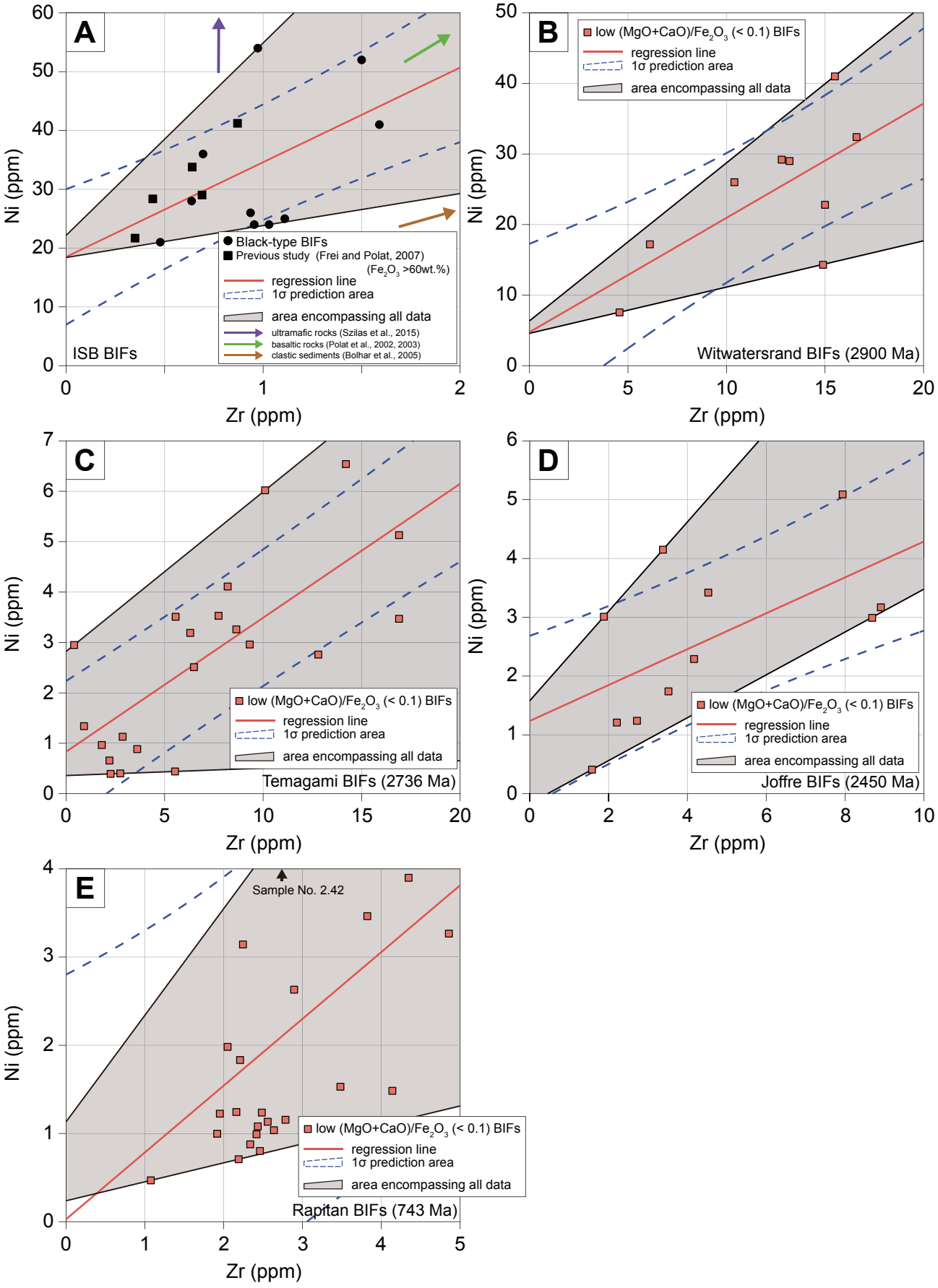

京都大学 KYOTO UNIVERSITY
A Self-archived copy in
Kyoto University Research Information Repository
https://repository.kulib.kyoto-u.ac.jp
京都大学学術情報リポジトリ KURENAI 紅 Kyoto University Research Information Repository



and transition metal contents basically increase with the iron contents, analogous to modern iron oxyhydroxides (German and Von Damm, 2003). However, all of the REE and transition elements, in fact, are not hosted by only the iron oxide minerals because the BIFs contain Ca- and Mg-bearing minerals as well as in negligible Zr and $Al_2O_3$ contents (Klein, 2005). The REEs, some transition elements of Co, Ni, Cu and Zn, alkaline earth metals of Sr and Ba, and HFSEs of Zr, Hf, U and Th are more abundant in Green-BIFs, and some White- and Gray-type BIFs than the Black-type BIFs at given $Fe_2O_3$ contents on their $Fe_2O_3$ variation diagrams and ternary plots (Figs. 6 and 8). The overabundance indicates that minerals rather than the iron oxides, which are abundant in the Green-, White- and Gray-type BIFs, also contain the elements. All of the BIFs in the ISB contain amphiboles, and especially the Green-type BIFs contain more amphiboles (Fig. 4F), consistent with higher Mg and Ca contents (Figs. 5 and 8). Because amphiboles, generally speaking, can host various elements except for HFSEs (e.g. Taylor and McLennan, 1985), the enrichment of some trace elements in the Mg- and Ca-rich BIFs of Green-type BIFs and some of White- and Gray-type BIFs are possibly due to the enrichment of amphiboles. The enrichment of those elements in amphibole-rich BIFs could be explained by two contrasting possibilities that Mg and Ca moved through metamorphic fluid during the metamorphism, or that Mg- and Ca-bearing materials such as silicates, carbonate and exhalative materials were involved during the deposition.

Firstly, we consider the possibility of metasomatism by Mg, Ca and Si-rich metamorphic fluid into the BIFs. Because the metamorphism fluid, generally speaking, is more enriched in LREE (Bau, 1993; Viehmann et al., 2015b), the Green-type BIFs should be more enriched in LREE than the Black-type BIFs. However, the involvement of metamorphic fluid is not consistent with the REE patterns because the formers have LREE-depleted REE patterns (Fig. 7).

Alternatively, we consider that the enrichment of those elements is due to involvement of carbonate minerals, silicate minerals, volcanic and detrital materials, from which the amphiboles were subsequently formed during the metamorphism. Although the involvement of calcite with/without dolomite does not result in amphibole formation under the greenschist facies condition, amphibole and calcite are formed through the reaction of quartz and dolomite, dependent on the $X_{CO_2}$, under the amphibolite facies condition (Spear, 1993). On the other hand, contamination of volcanic and clastic materials with a higher ratio of MgO to CaO leads to formation of amphibole under even the greenschist facies condition (Spear, 1993). Because they have shale-normalized LREE-depleted REE patterns, the contamination results in depletion of LREE in the BIFs, consistent with those of the Green-type BIFs (Fig. 7).

Despite of the cause of amphibole formation, the occurrence of the amphibole is not in favor of estimate of ancient seawater composition because the BIFs contain any materials besides iron oxyhydroxide.

A previous work used not only quartz–magnetite IFs but also magnesian IFs with a lot of amphiboles to estimate compositions of the Eoarchean seawater, and their BIF sample with the highest Ni/Fe ratio is the magnesian IF (10-2A, Dymek and Klein, 1988; Konhauser et al., 2009). If the contaminants are not clastic or volcanic detritus but silicate minerals of olivine and pyroxene, the contamination increases Ni contents but not Zr and $Al_2O_3$ contents because they do not contain Zr and $Al_2O_3$. Fig. 8F shows that Mg- and Ca-rich IFs are enriched in Ni relative to the iron-rich IFs. Because of significant influence of the Mg- and Ca-rich phases on whole rock compositions, only White-, Gray- and Black-type BIFs with low Mg and Ca contents ($(MgO + CaO)/Fe_2O_3 < 0.1$) are considered hereafter.

### 5.2. Influence of involvement of clastic and volcanic materials on whole-rock trace element contents

#### 5.2.1. Influence of their involvement on REE + Y and transitional element contents

Contamination of clastic and volcanic materials of silicate minerals, volcanic ashes and glass, and exhalative insoluble materials significantly disturbs seawater signatures of BIFs because the contaminants usually have higher REE, LILE, HFSE, and transition element contents (e.g. Bau, 1993). Generally speaking, $Al^{3+}$, $Ti^{4+}$, and HFSE are insoluble in aqueous solution (e.g. Martin and Whitfield, 1983; Andrews et al., 2004) and concentrated in clay minerals, weathering-resistant minerals such as zircon and some aluminous and titaniferous phases, REE-bearing minerals of monazite and apatite, volcanic glass and exhalative insoluble materials so that their abundances are often used as criteria for their involvement (e.g. Bau, 1993).

Previous works assumed the influence of involvement of clastic and volcanic materials on REE contents is negligible because Zr contents in their BIF samples are low, up to ca. 4.2 ppm (Bolhar et al., 2004), 10.2 ppm (Frei and Polat, 2007), ca. 2.2 ppm (Friend et al., 2008) and 3.1 ppm (Nutman et al., 2010). But, Fig. 9G displays that La contents are positively correlated with Zr contents even for Black- and White-type BIFs except for two Black-type BIFs (60B, 150B), and indicates that the LREE contents are influenced by the contaminants. The samples of 60B and 150B have relatively high $Al_2O_3$ (>1 wt.%) and HFSE (Zr > 2 ppm) contents. And their Pr, V and Ni contents are lower than others at a given Zr content but are higher than the minimum value of the Black-type BIFs at the low Zr content (Fig. 9A, C, G). The feature indicates that the samples are also influenced by the contamination but the contaminants have different compositions with high $Al_2O_3$, HFSE and U contents from others. Similar observation was previously reported by Frei and Polat (2007), who mentioned that highly LREE-enriched BIFs have higher Rb contents possibly due to contamination of detrital clay minerals. Some of our samples also have higher Rb contents than 2 ppm so that the samples with high Rb contents are eliminated possibly due to the involvement of clay minerals hereafter.

On the other hand, MREE and HREE contents are not well correlated with Zr contents, especially for the Black-type BIFs (Fig. 9H and I), suggesting that the contaminants have relatively low MREE and HREE contents. It is well known that Y and Ho, which share trivalent oxidation state and similar ionic radii, are not fractionated in magmatic systems, but Ho is preferentially scavenged by suspended particles relative to Y in aqueous systems. As a result, volcanic and clastic materials have almost chondritic values (ca. 26) whereas seawater and associated chemical sediments have

**Figure 10.** Zr variation diagrams of Ni contents: (A) BIFs in the ISB with low $Al_2O_3$ (<1 wt.%) and Rb (<2 ppm) contents and low $(MgO + CaO)/Fe_2O_3$ ratios (<0.1), including the magnetite-IFs (Frei and Polat, 2007), (B) 2900 Ma Witwatersrand iron formations, South Africa (Viehmann et al., 2015a), (C) 2736 Ma Temagami iron formations, Canada (Bau and Alexander, 2009), (D) 2450 Ma Joffre iron formations, Western Australia (Haugaard et al., 2016) with low $(MgO + CaO)/Fe_2O_3$ ratios (<0.1) and (E) 743 Ma Rapitan iron formations, Canada (Baldwin et al., 2012) with low $Al_2O_3$ (<1 wt.%), Zr contents (<10 ppm) and $(MgO + CaO)/Fe_2O_3$ ratios (<0.1). Blue, green and brown arrows mean the directions of compositions in ultramafic rocks, basaltic rocks and clastic sedimentary rocks in the ISB, respectively (Polat and Hofmann, 2003; Bolhar et al., 2005; Szilas et al., 2015). Red line and area enclosed with blue dotted line mean linear regression line and prediction area ($1\sigma$). Gray area mean are encompassing the all data.

京都大学 KYOTO UNIVERSITY
A Self-archived copy in
Kyoto University Research Information Repository
https://repository.kulib.kyoto-u.ac.jp
京都大学学術情報リポジトリ KURENAI 紅 Kyoto University Research Information Repository



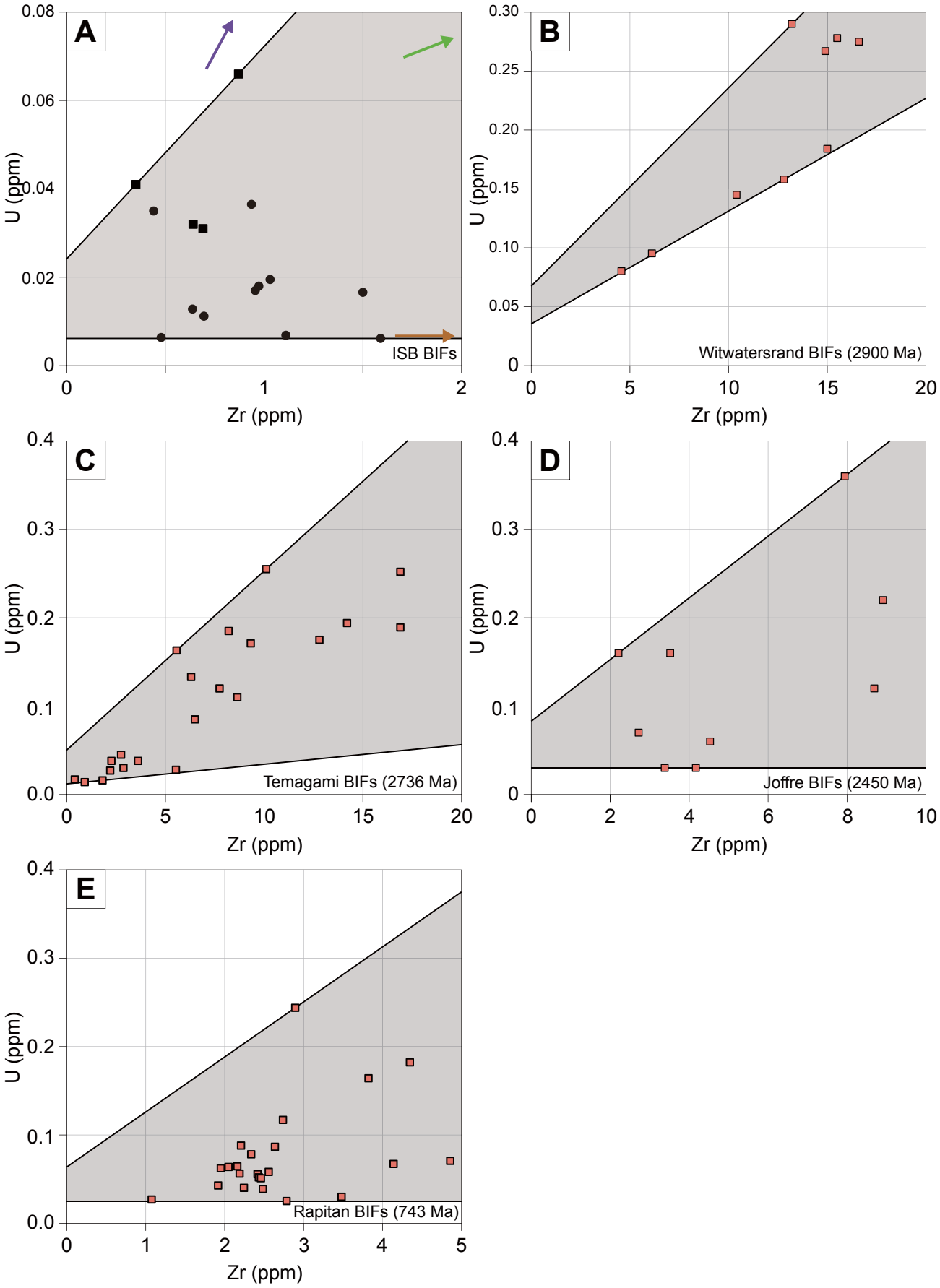


**Figure 11.** Zr variation diagrams of U contents: (A) BIFs in the ISB, (B) 2900 Ma Witwatersrand iron formations, South Africa, (C) 2736 Ma Temagami iron formations, Canada, (D) 2450 Ma Joffre iron formations, Western Australia and (E) 743 Ma Rapitan iron formations, Canada. The symbols are same as those in Fig. 10.

京都大学 KYOTO UNIVERSITY
A Self-archived copy in
Kyoto University Research Information Repository
https://repository.kulib.kyoto-u.ac.jp
京都大学学術情報リポジトリ KURENAI 紅 Kyoto University Research Information Repository



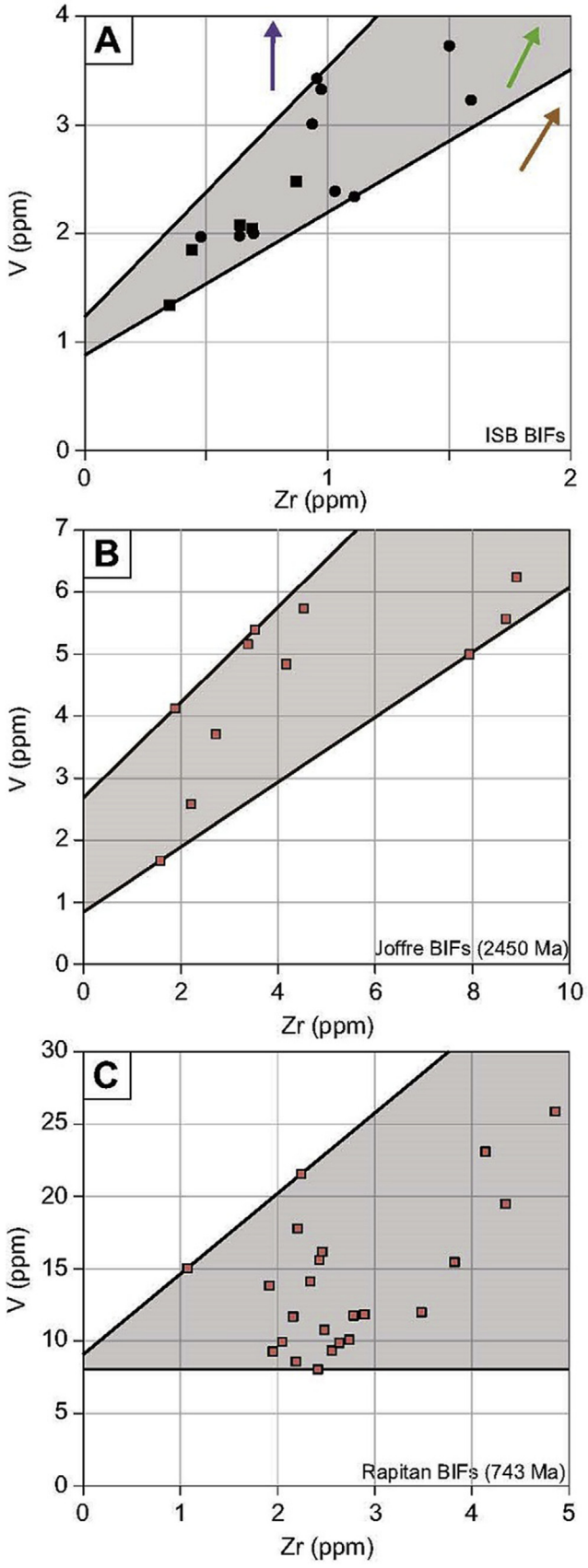


**Figure 12.** Zr variation diagrams of V contents: (A) BIFs in the ISB, (B) 2450 Ma Joffre iron formations, Western Australia and (C) 743 Ma Rapitan iron formations, Canada. The symbols are same as those in Fig. 10.

superchondritic Y/Ho ratios (e.g. Bau, 1996; Nozaki et al., 1997; Alibo and Nozaki, 1999; Bolhar et al., 2005). Contamination of clastic and volcanic materials depresses the Y/Ho ratios of chemical sediments, but all of our studied BIFs have higher Y/Ho ratios than the chondritic value, and lack a negative correlation between Zr content and Y/Ho ratios (Fig. 9K). The characteristics suggest that the influence of the contamination on the elements was insignificant for the Black-type BIFs.

### 5.2.2. Estimate of Ni, U and other transition elements of contamination-free BIFs

Konhauser and his colleagues suggested that the Archean ocean was enriched in Ni contents probably due to higher influx of hydrothermal fluids from Ni-rich komatiites because of higher Ni/Fe ratios of the Archean BIFs from 3.8 Ga to 2.7 Ga, and proposed that the high Ni contents resulted in prosperity of methanogens with a Ni-bearing key enzyme and depression of activity of oxygen-producing bacteria (Konhauser et al., 2009; Pecoits et al., 2009; Mloszewska et al., 2012, 2013). Konhauser et al. (2009) selected the BIFs with the low Ti, Zr, Th, Hf and Sc contents (<20 ppm) and Al contents ($Al_2O_3$ < 1%) to avoid the contamination of clastic materials. But, the transition element contents in the ISB BIFs, in fact, increase with the contaminations by the clastic and volcanic materials because “aluminous-graphitic IFs” with alumino-silicate minerals have higher contents of Al (0.57 wt.% < $Al_2O_3$ < 12.4 wt.%), HFSE (4.2 ppm < Zr < 94.7 ppm) and transitional elements (68.7 ppm < Ni < 230.3 ppm) relative to “quartz-magnetite IFs” (0.05 wt.% < $Al_2O_3$ < 2.66 wt.%, Zr < 21.9 ppm, 10.8 ppm < Ni < 48.6 ppm) (Dymek and Klein, 1988). In addition, this study shows that even low-Zr content (<2 ppm) samples have a positive correlation between Zr and Ni contents (Fig. 9C), and that the BIFs with higher Ca and Mg contents have the higher Ni/Fe ratios, as mentioned above. The facts indicate that the contamination more significantly influences on Ni contents of the BIFs than previously expected so that it is necessary to avoid the influence for estimate of ancient seawater composition. The Ni content of contamination-free BIFs can be ideally calculated from an intercept of a compositional variation of Ni contents on a Zr variation diagram, analogous to the modern iron oxyhydroxide (Sherrell et al., 1999). However, it is difficult to exactly determine another end-member(s) of the compositional variation, namely contaminant(s) because the compositional variation is more scattered at higher Zr contents. Therefore, we employed two methods to calculate the intercept. Firstly, assuming that the contaminant has only one component, the intercept was calculated from a regression line of all data of the Black-type BIFs with low Rb contents (<2 ppm) and magnetite-IFs with high iron contents ($Fe_2O_3$> 60 wt.%, Frei and Polat, 2007) to obtain 18 ± 12 ppm (Fig. 10A). Similar positive correlations are shown in younger BIFs. In the same way, the intercepts can be calculated to be 4.8 ± 13, 0.83 ± 1.4, 1.2 ± 1.4 and 0.028 ± 2.8 ppm for the 2.9, 2.7, 2.4 and 0.7 Ga BIFs, respectively (Fig. 10B–D). Secondly, the intercept was estimated from some regression lines covering all data of the Black-type BIFs and magnetite-IFs because the contaminants do not have only one composition but varied compositions, as mentioned above (Fig. 10A). The intercepts range from 18 to 22 for the ISB as well as from 4.5 to 7, from 0.36 to 2.8, from 0.16 to 1.6 and from 0.24 to 1.2 for the 2.9, 2.7, 2.4 and 0.7 Ga BIFs, respectively (Fig. 10B–E). Because the contaminants are highly varied, for example silicate minerals of olivine and pyroxene, clastic, volcanic, ultramafic and exhalative materials, carbonate minerals and clay minerals, it is considered that the latter method can obtain the compositions of contamination-free BIFs more accurately.

The uranium content of the contamination-free BIF can be also estimated from the Zr vs. U content diagram, analogous to the Ni contents of the contamination-free BIFs. A positive

京都大学 KYOTO UNIVERSITY
A Self-archived copy in
Kyoto University Research Information Repository
https://repository.kulib.kyoto-u.ac.jp
京都大学学術情報リポジトリ KURENAI 紅 Kyoto University Research Information Repository



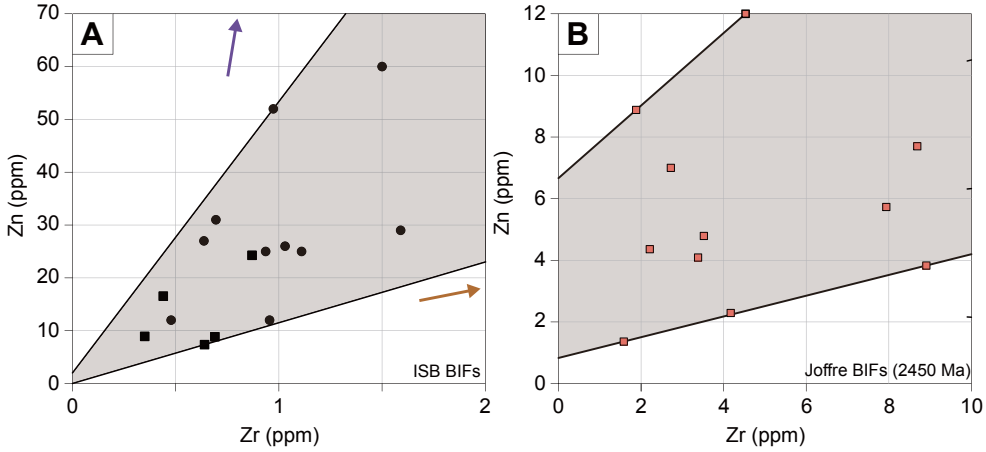


**Figure 13.** Zr variation diagrams of Zn contents: (A) BIFs in the ISB and (B) 2450 Ma Joffre iron formations, Western Australia. The symbols are same as those in Fig. 10.

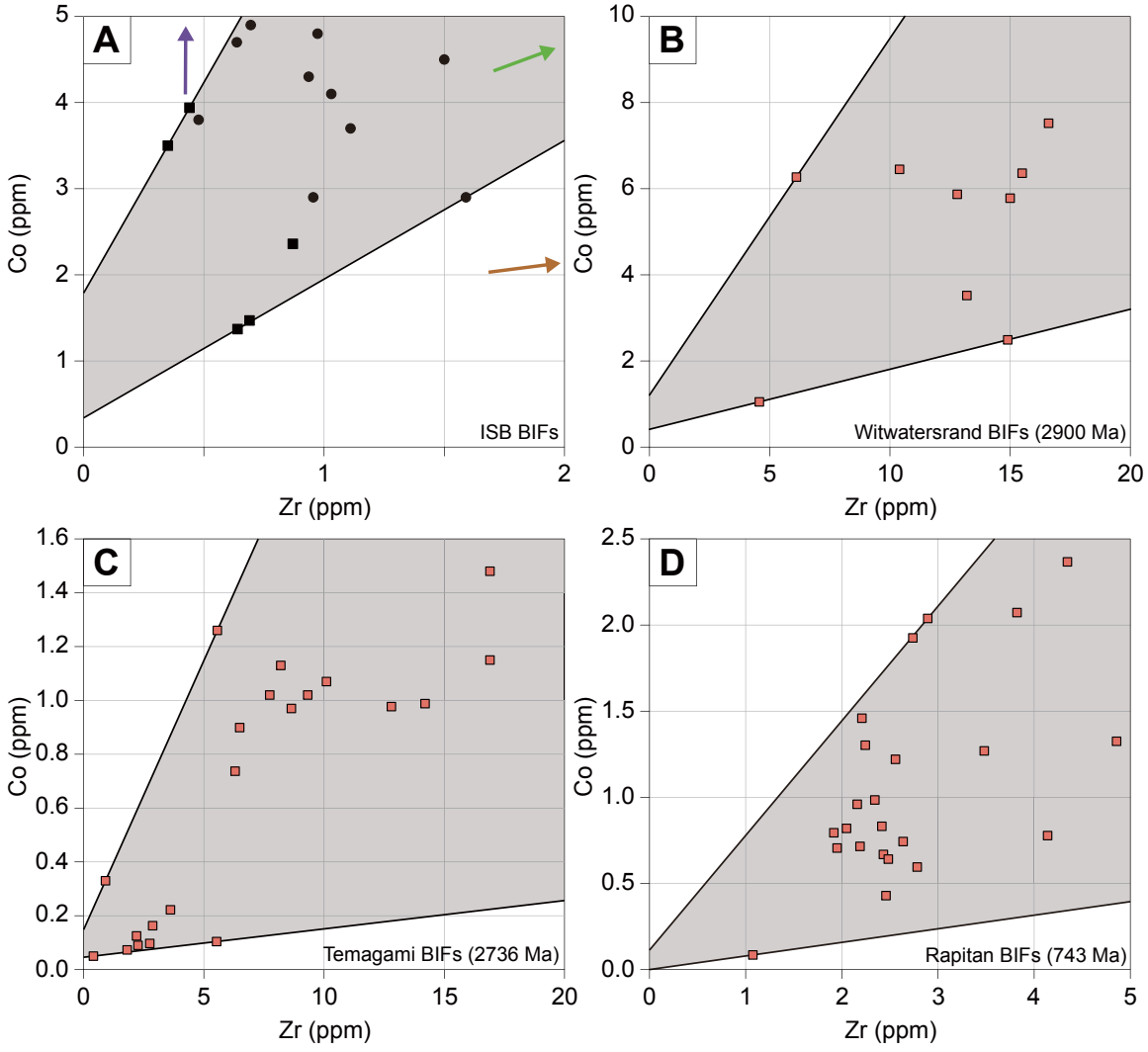


**Figure 14.** Zr variation diagrams of Co contents: (A) BIFs in the ISB, (B) 2900 Ma Witwatersrand iron formations, South Africa, (C) 2736 Ma Temagami iron formations, Canada, and (D) 743 Ma Rapitan iron formations, Canada. The symbols are same as those in Fig. 10.

京都大学 KYOTO UNIVERSITY
A Self-archived copy in
Kyoto University Research Information Repository
https://repository.kulib.kyoto-u.ac.jp
京都大学学術情報リポジトリ KURENAI 紅 Kyoto University Research Information Repository



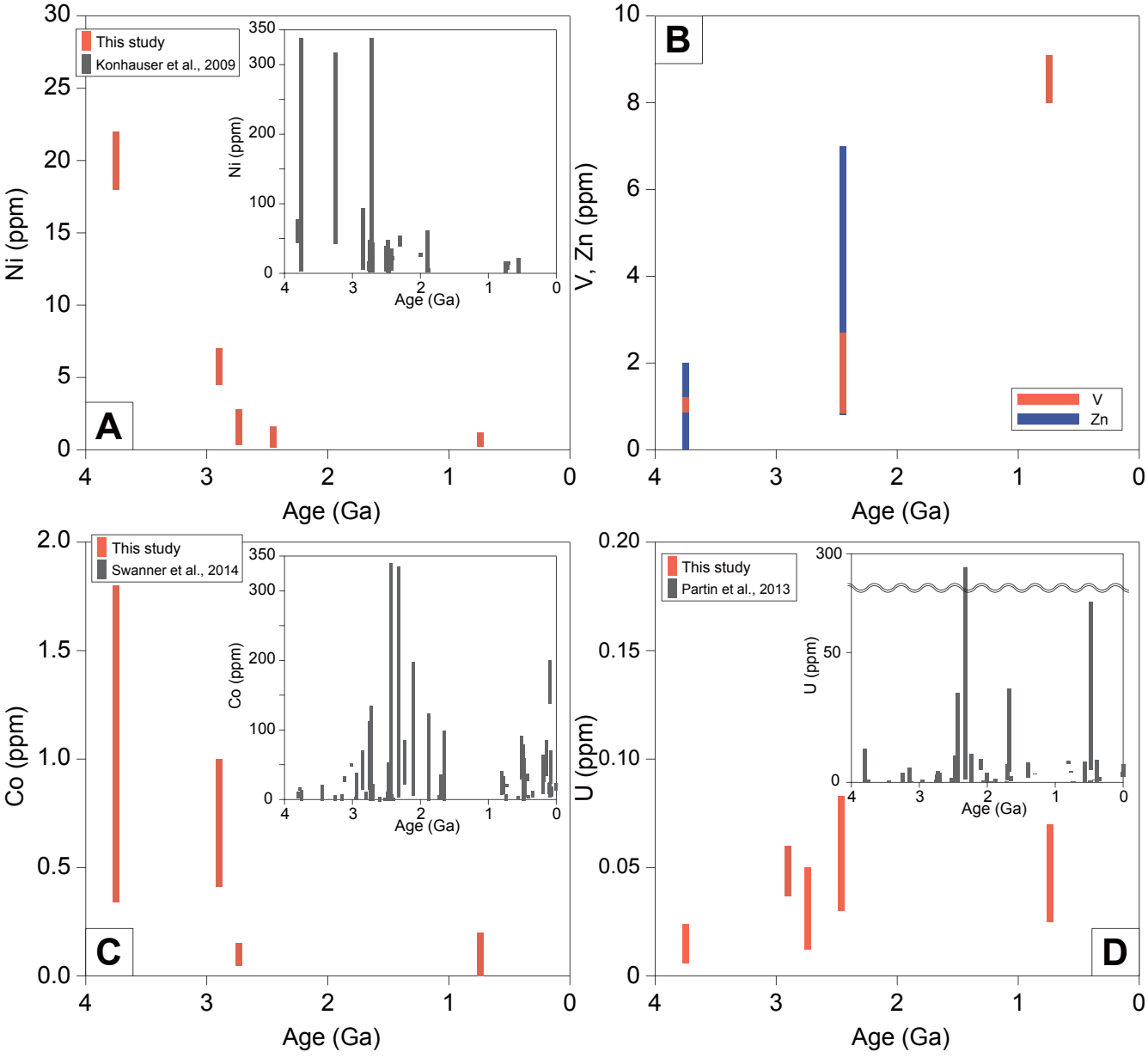


**Figure 15.** Secular variations of (A) Ni, (B) V and Zn, (C) Co and (D) U contents. The inlet figures show compilations of BIF compositions for Ni (Konhauser et al., 2009), Co (Swanner et al., 2014) and U (Partin et al., 2013), respectively.

correlation of U contents with Zr contents for the Isua BIFs also indicate contamination-free BIFs have less uranium contents, and the U content is estimated to be from 0.0061 to 0.024 by the second method (Figs. 9J and 11A). Partin et al. (2013) excluded BIF samples in the ISB and Nuvvuagittuq Supracrustal Belt (NSB) from their compilation because they considered that severely metamorphosed rocks less likely preserve a seawater signature of uranium content possibly due to late remobilization of uranium. In fact, some of them have significantly high U contents, up to 0.79 ppm and 23.4 ppm for ISB and NSB, repetitively. But, the BIFs also show positive correlations of U contents with $Al_2O_3$ contents, and the minimum values are 0.04 ppm and 0.02 ppm at the lowest $Al_2O_3$ contents for the ISB and NSB, respectively, so that the apparent high uranium contents can be explained by involvement of U-bearing contaminants. On the other hand, the U contents of contamination-free BIFs with low MgO and CaO contents ((CaO + MgO)/FeO < 0.1)) were estimated to be from 0.037 to 0.06, from 0.012 to 0.050, from 0.030 to 0.083 and from 0.025 to 0.07 ppm for 2.9, 2.7, 2.4 and 0.7 Ga BIFs based on the correlations of U contents with Zr contents, respectively (Fig. 11B–D).

Similarly, the vanadium contents of the BIFs are also correlated with Zr contents so that the variation is at least partially due to the involvement of the clastic and volcanic materials (Fig. 9A). The V contents of contamination-free BIFs are estimated to range from 0.88 ppm to 1.2 ppm for the ISB BIFs, from 0.84 ppm to 2.7 ppm at 2.4 Ga and from 8.0 ppm to 9.1 ppm at 0.7 Ga, respectively (Fig. 12).

Zinc also displays a positive correlation with Zr contents for the Black-type BIFs, and the Zn contents of the contamination-free BIFs are estimated to be from 0 to 2 ppm at ca. 3.8 Ga, and from 0.8 ppm to 7 ppm at 2.4 Ga at 0 ppm in Zr contents (Fig. 13). Cobalt contents in the Black-type BIFs with low Rb contents (<2 ppm) and

京都大学 KYOTO UNIVERSITY
A Self-archived copy in
Kyoto University Research Information Repository
https://repository.kulib.kyoto-u.ac.jp
京都大学学術情報リポジトリ KURENAI 紅 Kyoto University Research Information Repository



magnetite-IF ($Fe_2O_3$ > 60 wt.%) also form a positive correlation against Zr contents so that we can estimate the Co content of a contamination-free BIF from 0.34 ppm to 1.8 ppm (Fig. 14). In the same way, the Co contents are estimated to be from 0.41 ppm to 1 ppm, from 0.046 ppm to 0.15 ppm and from 0 to 0.2 ppm at 2.9, 2.7 and 0.7 Ga, respectively (Fig. 14).

The secular changes of the vanadium, zinc and cobalt contents of contamination-free BIFs show the vanadium and zinc contents increased whereas the cobalt content through the time (Fig. 15B and C).

Other transition elements such as copper show no clear positive correlations with Zr contents (Fig. 9D), suggesting that minimal effects of the clastic and volcanic contaminations or highly variable compositions in the contaminants. The copper contents of the BIFs are highly scattered from 1.3 to 5.7 even for the Black-type BIFs (Fig. 9D). Although the Isua BIFs have low modal abundances of sulfide minerals, a few sulfide grains are found in some Isua BIFs (e.g. Mojzsis et al., 2003; Dauphas et al., 2007; Yoshiya et al., 2015). The scattering is possibly due to involvement of sulfides into the BIFs for the enrichment or early deposition of the sulfide around hydrothermal vents, analogous to modern ferruginous sediments for depletion (German and Von Damm, 2003), respectively.

#### 5.2.3. Trace element compositions of cherts and interference of silica absorption in the transient element contents in the BIF

The amounts of Ni adsorbed on iron oxyhydroxide depend on not only Ni contents of seawater but also other compositions like Si contents (e.g. Konhauser et al., 2009). The Ni contents of the BIFs are well correlated with $Fe_2O_3$ contents because cherts and siliceous BIFs have lower Ni contents due to dilution of silica minerals (Fig. 6C). But, looking closely, there is an obvious gap of the Ni contents between the White- and Black-type BIFs (Figs. 6C and 9C). The gap is more obvious for V contents (Figs. 6A and 9A). Hindrance of adsorption of Ni on the iron-oxyhydroxide by dissolved Si possibly accounts for the obvious Ni-depletion in the cherts and siliceous BIFs. The apparent gap of Ni contents between the White- (siliceous) and Black-type (magnetite-dominant) BIFs suggests that the interference by the dissolved Si are more significant for the precipitation of the White-type BIFs whereas played an insignificant role on the Black-type BIFs possibly because the silica was under-saturated during the deposition of Black-type BIFs due to higher dissolved iron contents. The characteristics that the gap for V contents on the $Fe_2O_3$ and Zr variation diagrams are larger than for Ni contents can be explained by the difference in degree of adsorption of Ni and V on iron hydroxide (Li, 1981, 1982; Hein et al., 2000; Hein et al., 2003; Takahashi et al., 2015). The vanadium is more effectively influenced by the interference of silica.

### 5.3. Evolution of transition element contents of seawater throughout the time

Fig. 15 shows secular changes of V, Co, Ni, Zn and U contents of contamination-free BIFs through geologic time. The Ni and Co contents decrease whereas the V, Zn and U contents increase through the time. It is widely accepted that methanogen is one of the earliest microbial activity on the Earth (e.g. Takai et al., 2006), and possibly played important roles on the surface environment because it is considered that the emergence of the methanogen supplied methane to compensate faint luminosity of the young Sun (Pavlov et al., 2000) and higher activity of the methanogen prevented oxidation of surface environment by oxygen-producing bacteria (Konhauser et al., 2009). Nickel is a bio-essential element for the methanogen because the nickel is held in a heterocyclic ring of an enzyme methyl coenzyme M reductase, Cofactor F430 (Jaun and Thauer, 2007; Ragdale, 2014). Konhauser et al. (2009) showed secular change of Ni contents of the BIFs through the time, and proposed that methanogen had flourished before the Great Oxidation Event around 2.4 Ga because the seawater was enriched in Ni contents and that depression of methanogen activity due to decrease in the Ni content of seawater resulted in increase of atmospheric oxygen. Fig. 15A shows a secular change of Ni contents of contamination-free BIFs through the time. The Archean iron deposits have slightly higher Ni contents than the post-Archean equivalents but much lower than previously estimated (Konhauser et al., 2009). In addition, the Ni contents apparently decreased in the Mesoarchean (ca. 2.7 Ga) rather than the Great Oxidation Event, inconsistent with the idea that the decrease in Ni contents of seawater caused the Great Oxidation Event through decline of methanogen activity. If the Ni content of seawater controlled the activity of methanogens, the activity declined from ca. 2.9 Ga to 2.7 Ga. Recently, some geochemical evidence suggested that the emergence and prosperity of oxygen-producing bacteria have already occurred around 2.7–3.0 Ga based on REE contents and Ce anomalies of carbonate minerals (Komiya et al., 2008), Fe isotopes of sulfides in carbonate rocks (Nishizawa et al., 2010) and Mo isotopes of the BIFs (Planavsky et al., 2014). The decline of dissolved Ni contents in seawater before 2.7 Ga is possibly related with the emergence of oxygen-producing bacteria.

Uranium has four valences, $U^{3+}$, $U^{4+}$, $U^{5+}$ and $U^{6+}$, and forms an insoluble uranium oxide, uraninite, under reduced condition whereas forms soluble oxoacid and carbonate complexes under the oxic condition. The presence of uraninite in the clastic sedimentary rocks is considered as evidence for anoxic atmosphere until the Late Archean (e.g. Holland, 1994). Partin et al. (2013) compiled molar U/Fe ratios and U contents of the BIFs throughout the Earth history, and showed they increased up to $2.4 \times 10^{-6}$ and ca. 400 ppm around 2.32 Ga in the Great Oxidation Event (GOE). They discussed that delivery of $U^{6+}$ to ocean was increased due to oxidative continental weathering. The secular change of the uranium contents of the BIFs shows the uranium content stated to increase at least in the late Archean (Fig. 15D). The increase is possibly due to abrupt increase of continental growth and oxidative continental weathering because geological, geochemical and geobiological evidence suggests increase in oxygen content of seawater in the Late Archean (Hayes, 1994; Eigenbrode et al., 2008; Komiya et al., 2008; Bosak et al., 2009; Yoshiya et al., 2012). Our reconstructed secular change of uranium contents of BIFs supports $U^{4+}$ oxidation around 2.9 Ga to 2.7 Ga, suggested by lower Th/U ratios in the BIFs than an average continental crust value (Bau and Alexander, 2009).

Vanadium varies from +2 to +5 in the valance, is soluble as various vanadate compounds under oxic condition, and one of bioessential elements for some nitrogen-fixing microorganisms such as Azotobacter, algae and some metazoans of ascidians (e.g. Sigel and Sigel, 1995). Our estimate of secular variation of vanadium contents of BIFs indicates that the vanadium content of BIFs increased in the Late Archean (Fig. 15B), and suggests that dissolved vanadate influx into ocean possibly increased with increasing of oxidative continental weathering, analogous to the U contents. On the other hand, zinc occurs only as a divalent ion in natural environments, and is fixed as sulfide minerals under the sulfidic condition. It is well known that Zn is used for metallopeptidases, metallophosphatases and many other polymerases involved in DNA- and RNA-binding and synthesis (Liscomb and Sträter, 1996). Our estimate of secular variation of Zn contents shows Zn contents of the BIFs increased in the Late Archean, and suggests that the Zr content of seawater increased since then, similar to the U and V contents (Fig. 15B).

京都大学 KYOTO UNIVERSITY
A Self-archived copy in
Kyoto University Research Information Repository
https://repository.kulib.kyoto-u.ac.jp
京都大学学術情報リポジトリ KURENAI 紅 Kyoto University Research Information Repository



Cobalt has +2 and + 3 in the valence, and is also soluble as a divalent ion under the reducing environment, whereas oxidized and fixed as an insoluble trivalent ion by manganese deposits under the oxic condition. Cobalt is also one of the bioessential elements, and, for example, is involved in a vitamin B12 for synthesis of methionine. Swanner et al. (2014) compiled Co/Ti ratios of the BIFs through the time, and showed that the ratio increased from ca. 2.8 to 1.8 Ga. They interpreted that the seawater was enriched in the Co content at that time due to high hydrothermal influx and low Co burial efflux. On the other hand, our result show the Co content decreased though the time (Fig. 15C).

### 5.4. Correlations of stratigraphy with Y/Ho ratios and Eu anomaly

Fig. 16A shows an obvious correlation of Y/Ho ratios of the BIFs with the stratigraphic positions. All of the BIFs have higher Y/Ho ratios than a chondritic value (ca. 26), PAAS (ca. 27), an Archean mudstone (ca. 24, Taylor and McLennan, 1985), modern river waters (ca. 38, Nozaki et al., 1997) and modern hydrothermal fluid (ca. 32, Bau and Dulski, 1999), and similar values to modern seawaters from 43 to 80 (Nozaki et al., 1997). The Y/Ho ratios in Archean chemical sedimentary rocks are often used as a proxy of balance between seawater and hydrothermal fluid in a depositional environment (e.g. Alexander et al., 2008). The stratigraphically increasing trend of the Y/Ho ratios in the BIFs suggests that a seawater-like component with a high Y/Ho ratio increase progressively in the depositional environments of the BIFs.

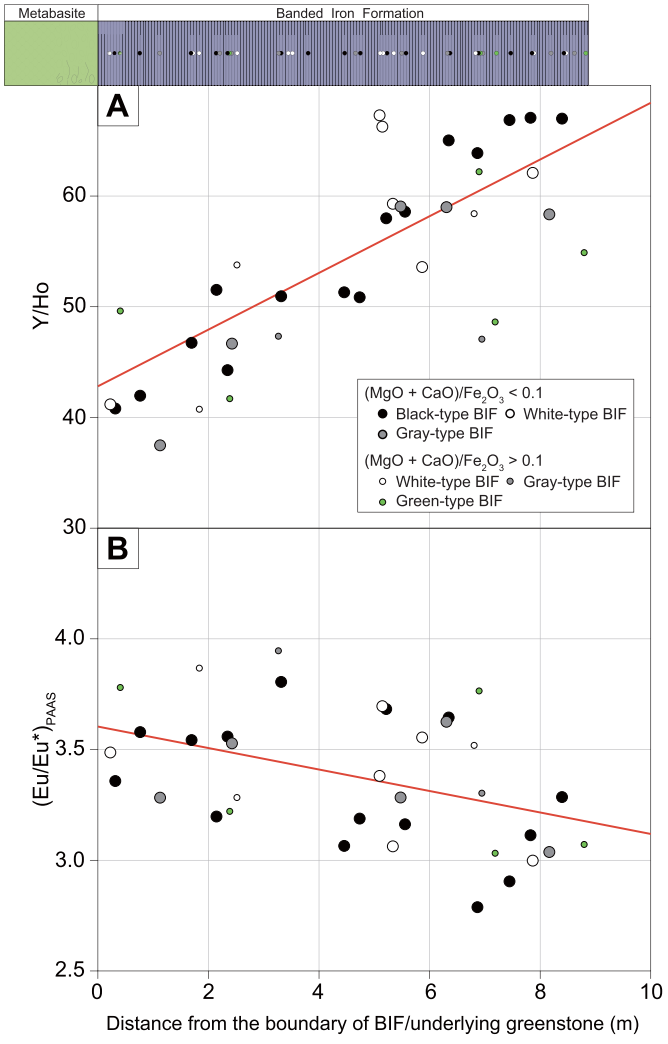


**Figure 16.** Correlations of (A) Y/Ho ratios and (B) positive Eu anomalies with the stratigraphic positions from the underlying basaltic lavas (Fig. 2).

Fig. 16B shows relationship of the positive Eu anomalies of the BIFs with stratigraphic positions. Although more scattered than Y/Ho ratios, the positive Eu anomalies obviously decrease with increasing stratigraphic positions. Because modern hydrothermal fluids have distinct positive Eu anomalies in shale-normalized REE patterns (e.g. Klinkhammer et al., 1994; Bau and Dulski, 1999; German and Von Damm, 2003), the stratigraphically upward trend of Eu anomaly can be explained by decrease of a hydrothermal fluid component in the BIFs. Alternatively, decrease of high-temperature hydrothermal fluid component also accounts for the stratigraphically upward trend because the positive Eu anomaly is unique to high temperature (>300 °C) hydrothermal fluids (e.g. Klinkhammer et al., 1994). However, increase of high-temperature hydrothermal fluid leads to higher influx of Fe and Mn compared with low-temperature components of Si, Ba and Ca so that REE and Ni contents adhering to the iron oxyhydroxide would decrease due to higher precipitation rates of iron oxyhydroxide. Because the REE and Ni contents are not correlated with the stratigraphic position, the former model is capable of explaining the stratigraphically upward trend.

Generally speaking, BIFs comprise two components of iron oxyhydroxide and silica, and they, at present, are transformed to magnetite and quartz in the ISB, respectively. A Nd isotope variation of black and white bands within a slabbed BIF sample shows that the black bands have higher Nd isotope values and higher positive Eu anomalies than the white bands, and suggests that the black bands have more hydrothermal components than the white bands (Frei and Polat, 2007). The geochemical difference that the BIFs have higher silicon isotope values and higher positive Eu anomalies than cherts also suggest that the BIFs contain more hydrothermal components than chert (André et al., 2006). However, the stratigraphic upward trends of the Y/Ho ratios and positive Eu anomalies are inconsistent with the Nd and Si isotopes at a glance because the stratigraphic upward trends of Y/Ho ratios and positive Eu anomalies are apparently independent of their lithologies. However, it is considered that the Nd isotope variation of the BIF sample reflects variations within hydrothermal plumes in a short term because it was obtained from only ca. 10 cm long part of a BIF sequence. On the other hand, because our stratigraphic upward trends were obtained from almost the whole BIF sequence, the trends indicate the temporal change through the BIF deposition.

It is well known that a modern drilled metalliferous sedimentary sequence around the East Pacific Rise (EPR) also displays that positive Eu anomalies decrease with the stratigraphy upwards (Ruhlin and Owen, 1986; Olivarez and Owen, 1991). The compositional change of the EPR metalliferous sediments can be explained by decrease in ratios of hydrothermal to seawater components with increasing distance from a ridge axis through ocean plate movement. The upward decrease of the positive Eu anomalies was also reported from the Mesoarchean BIFs in the Cleaverville area of the Pilbara craton, Western Australia, and was explained by change of depositional setting from mid-ocean ridge to continental margin (Kato et al., 1998). The stratigraphic upward trends of Y/Ho ratios and positive Eu anomalies of the BIFs in the ISB are also accounted for by change of depositional setting, analogous to the modern and Mesoarchean metalliferous sediments, and supports the ocean plate stratigraphy and possible accretionary complex model for the formation of the ISB (Komiya et al., 1999; Furnes et al., 2007). Because the greenstones have arc-affinity signatures such as Nb-depletion in the ISB (Polat et al., 2002; Dilek and Polat, 2008; Furnes et al., 2014), the ridge axis

京都大学 KYOTO UNIVERSITY
A Self-archived copy in
Kyoto University Research Information Repository
https://repository.kulib.kyoto-u.ac.jp
京都大学学術情報リポジトリ KURENAI 紅 Kyoto University Research Information Repository



would be located in the suprasubduction setting (Komiya et al., 2015). On the other hand, recent reappraisal of the Nb-poor greenstones suggests that the Nb-depletion was partially due to crustal contamination or later metasomatism of Nb-poor fluids (Hoffmann et al., 2010). Further comprehensive studies should be necessary to determine the tectonic setting of the Isua supracrustal belt.

## 6. Conclusions

We petrographically classified BIFs in the Isua supracrustal belt into four types: Black-, Gray-, Green- and White-types, respectively. The amphibole-rich Green-type BIFs were enriched in REE + Y and transitional elements due to contamination of Mg- and Ca-bearing minerals so that they are unsuitable for the estimate of seawater composition.

The magnetite-rich Black-type BIFs show positive correlations of LREE, transitional element (V, Co, Ni, Zn and U) contents with Zr contents, suggesting that the compositions also suffered from contaminations of volcanic, clastic and exhalative materials. Similar correlations are observed for 2.9, 2.7, 2.4 and 0.7 Ga BIFs. Nickel content of contamination-free BIFs in the Eoarchean, which is calculated from an intercept of a compositional variation of their contents on a Zr variation diagram, is much lower than previously estimated. Our reconstructed secular variation of Ni contents of BIFs shows that the Ni content had already decreased before 2.7 Ga, in contrast to previous works. We also reconstructed secular variations of V, Co, Zn and U contents of BIFs through the time, which shows Ni and Co contents decreased whereas V, Zn and U contents increased through the time. Especially, the Ni and Co contents drastically decreased in the Mesoarchean whereas the V, Zn and U contents progressively increased from the Mesoarchean to the Proterozoic.

The BIFs increased in Y/Ho ratios and decreased in positive Eu anomalies stratigraphical upwards, analogous to modern metalliferous sediments on the spreading oceanic plate. The similarities suggest that the REE + Y stratigraphic variations of the BIFs can be also explained by decreasing of ratios of hydrothermal to seawater components with increasing distance from a middle oceanic ridge due to movement of oceanic plate. It supports the existence of ocean plate stratigraphy and an accretionary complex in the ISB as well as the Eoarchean plate tectonics.

## Acknowledgments

We thank Prof. Shigenori Maruyama, who provides opportunity to publish this study. We wish to thank Prof. Shigenori Maruyama, Toshiaki Masuda and Peter Appel for geological survey in the Isua supracrustal belt. Many fruitful comments by Dr. Viehmann improved the manuscript. This research was partially supported by JSPS grants (No. 26220713) from the Ministry of Education, Culture, Sports, Science and Technology of Japan.

## Appendix A. Supplementary data

Supplementary data related to this article can be found at http://dx.doi.org/10.1016/j.gsf.2016.11.016.

## References

Alibo, D.S., Nozaki, Y., 1999. Rare earth elements in seawater: particle association, shale-normalization, and Ce oxidation. Geochimica et Cosmochimica Acta 63, 363–372.
Alexander, B.W., Bau, M., Andersson, P., Dulski, P., 2008. Continentally-derived solutes in shallow Archean seawater: rare earth element and Nd isotope evidence in iron formation from the 2.9 Ga Pongola Supergroup. South Africa/Geochimica et Cosmochimica Acta 72, 378–394.
Allaart, J.H., 1976. The Pre-3760 m.y. old supracrustal rocks of the Isua area, central West Greenland, and the associated occurrence of quartz-banded ironstone. In: Windley, B.F. (Ed.), The Early History of the Earth. John Wiley & Sons, London, pp. 177–189.
André, L., Cardinal, D., Alleman, L.Y., Moorbath, S., 2006. Silicon isotopes in ~3.8 Ga West Greenland rocks as clues to the Eoarchaean supracrustal Si cycle. Earth and Planetary Science Letters 245, 162–173.
Andrews, J.E., Brimblecombe, P., Jickells, T.D., Liss, P.S., Reid, B., 2004. An Introduction to Environmental Chemistry, second ed. Blackwell Science, Malden, USA. 296 pp.
Appel, P.W.U., 1980. On the early Archaean Isua iron-formation, West Greenland. Precambrian Research 11, 73–87.
Appel, P.W.U., Fedo, C.M., Moorbath, S., Myers, J.S., 1998. Recognizable primary volcanic and sedimentary features in a low-strain domain of the highly deformed, oldest known (≈ 3.7–3.8 Gyr) Greenstone Belt, Isua, West Greenland. Terra Nova 10, 57–62.
Arai, T., Omori, S., Komiya, T., Maruyama, S., 2015. Intermediate P/T-type regional metamorphism of the Isua supracrustal belt, southern West Greenland: the oldest Pacific-type orogenic belt? Tectonophysics 662, 22–39.
Baldwin, G.J., Turner, E.C., Kamber, B.S., 2012. A new depositional model for glaciogenic Neoproterozoic iron formation: insights from the chemostratigraphy and basin configuration of the Rapitan iron formation 1 Northwest Territories Geoscience Office Contribution 0052. Canadian Journal of Earth Sciences 49, 455–476.
Bau, M., 1993. Effects of syn- and post-depositional processes on the rare-earth element distribution in Precambrian iron-formations. European Journal of Mineralogy 5, 257–267.
Bau, M., 1996. Controls on the fractionation of isovalent trace elements in magmatic and aqueous systems: evidence from Y/Ho, Zr/Hf, and lanthanide tetrad effect. Contributions to Mineralogy and Petrology 123, 323–333.
Bau, M., Dulski, P., 1996. Distribution of yttrium and rare-earth elements in the Penge and Kuruman iron-formations, Transvaal Supergroup, South Africa. Precambrian Research 79, 37–55.
Bau, M., Dulski, P., 1999. Comparing yttrium and rare earths in hydrothermal fluids from the mid-Atlantic ridge: implications for Y and REE behaviour during near-vent mixing and for the Y/Ho ratio of Proterozoic seawater. Chemical Geology 155, 77–90.
Bau, M., Alexander, B.W., 2009. Distribution of high field strength elements (Y, Zr, REE, Hf, Ta, Th, U) in adjacent magnetite and chert bands and in reference standards FeR-3 and FeR-4 from the Temagami iron-formation, Canada, and the redox level of the Neoarchean ocean. Precambrian Research 174, 337–346.
Bjerrum, C.J., Canfield, D.E., 2002. Ocean productivity before about 1.9 Gyr ago limited by phosphorus adsorption onto iron oxides. Nature 417, 159–162.
Bolhar, R., Kamber, B.S., Moorbath, S., Fedo, C.M., Whitehouse, M.J., 2004. Characterisation of early Archaean chemical sediments by trace element signatures. Earth and Planetary Science Letters 222, 43–60.
Bolhar, R., Kamber, B.S., Moorbath, S., Whitehouse, M.J., Collerson, K.D., 2005. Chemical characterization of Earth's most ancient clastic metasediments from the Isua Greenstone Belt, southern West Greenland. Geochimica et Cosmochimica Acta 69, 1555–1573.
Bosak, T., Liang, B., Sim, M.S., Petroff, A.P., 2009. Morphological record of oxygenic photosynthesis in conical stromatolites. Proceedings of the National Academy of Sciences 106, 10939–10943. http://dx.doi.org/10.1073/pnas.0900885106.
Crowley, J.L., Myers, J.S., Dunning, G.R., 2002. Timing and nature of multiple 3700-3600 Ma tectonic events in intrusive rocks north of the Isua Greenstone Belt, southern West Greenland. Geological Society of America Bulletin 114, 1311–1325.
Crowley, J.L., 2003. U–Pb geochronology of 3810–3630 Ma granitoid rocks south of the Isua Greenstone Belt, southern West Greenland. Precambrian Research 126, 235–257.
Dauphas, N., van Zuilen, M., Wadhwa, M., Davis, A.M., Marty, B., Janney, P.E., 2004. Clues from Fe isotope variations on the origin of Early Archean BIFs from Greenland. Science 306, 2077–2080.
Dauphas, N., van Zuilen, M., Busigny, V., Lepland, A., Wadhwa, M., Janney, P.E., 2007. Iron isotope, major and trace element characterization of early Archean supracrustal rocks from SW Greenland: protolith identification and metamorphic overprint. Geochimica et Cosmochimica Acta 71, 4745–4770.
Dilek, Y., Polat, A., 2008. Suprasubduction zone ophiolites and Archean tectonics. Geology 36, 431–432.
Dulski, P., 2001. Reference materials for geochemical studies: new analytical data by ICP–MS and critical discussion of reference values. Geostandards Newsletter 25, 87–125.
Dymek, R.F., Klein, C., 1988. Chemistry, petrology and origin of banded iron-formation lithologies from the 3800 Ma Isua supracrustal belt, West Greenland. Precambrian Research 39, 247–302.
Eggins, S.M., Woodhead, J.D., Kinsley, L.P.J., Mortimer, G.E., Sylvester, P., McCulloch, M.T., Hergt, J.M., Handler, M.R., 1997. A simple method for the precise determination of ≥ 40 trace elements in geological samples by ICPMS using enriched isotope internal standardisation. Chemical Geology 134, 311–326.
Eigenbrode, J.L., Freeman, K.H., Summons, R.E., 2008. Methylhopane biomarker hydrocarbons in Hamersley Province sediments provide evidence for Neoarchean aerobiosis. Earth and Planetary Science Letters 273, 323–331.

京都大学 KYOTO UNIVERSITY
A Self-archived copy in
Kyoto University Research Information Repository
https://repository.kulib.kyoto-u.ac.jp
京都大学学術情報リポジトリ KURENAI 紅 Kyoto University Research Information Repository



Frei, R., Bridgwater, D., Rosing, M.T., Stecher, O., 1999. Controversial Pb-Pb and Sm-Nd isotope results in the early Archean Isua (West Greenland) oxide iron formation: preservation of primary signatures versus secondary disturbances. Geochimica et Cosmochimica Acta 63, 473–488.

Frei, R., Polat, A., 2007. Source heterogeneity for the major components of ~ 3.7 Ga banded iron formations (Isua Greenstone Belt, Western Greenland): tracing the nature of interacting water masses in BIF formation. Earth and Planetary Science Letters 253, 266–281.

Friend, C.R.L., Nutman, A.P., McGregor, V.R., 1988. Late Archaean terrane accretion in the Godthåb region, southern West Greenland. Nature 335, 535–538.

Friend, C.R.L., Nutman, A.P., Bennett, V.C., Norman, M.D., 2008. Seawater-like trace element signatures (REE + Y) of Eoarchaean chemical sedimentary rocks from southern West Greenland, and their corruption during high-grade metamorphism. Contributions to Mineralogy and Petrology 155, 229–246.

Furnes, H., de Wit, M., Staudigel, H., Rosing, M., Muehlenbachs, K., 2007. A vestige of Earth's oldest ophiolite. Science 315, 1704–1707.

Furnes, H., Rosing, M., Dilek, Y., de Wit, M., 2009. Isua supracrustal belt (Greenland)-a vestige of a 3.8 Ga suprasubduction zone ophiolite, and the implications for Archean geology. Lithos 113, 115–132.

Furnes, H., de Wit, M., Dilek, Y., 2014. Four billion years of ophiolites reveal secular trends in oceanic crust formation. Geoscience Frontiers 5, 571–603.

German, C.R., Von Damm, K.L., 2003. Hydrothermal processes, the oceans and marine geochemistry. In: Holland, H.D., Turekian, K.K. (Eds.), Treatise on Geochemistry, vol. 6. Elsevier-Pergamon, Oxford, pp. 181–222.

Haugaard, R., Pecoits, E., Lalonde, S., Rouxel, O., Konhauser, K., 2016. The Joffre banded iron formation, Hamersley Group, Western Australia: assessing the palaeoenvironment through detailed petrology and chemostratigraphy. Precambrian Research 273, 12–37.

Hayashi, M., Komiya, T., Nakamura, Y., Maruyama, S., 2000. Archean regional metamorphism of the Isua supracrustal belt southern West Greenland: implications for a driving force for Archean plate tectonics. International Geology Review 42, 1055–1115.

Hayes, J.M., 1994. Global methanotrophy at the Archean-Proterozoic transition. In: Bengtson, S. (Ed.), Early Life on Earth. Columbia University Press, New York, pp. 220–236.

Hein, J.R., Koschinsky, A., Bau, M., Manheim, F.T., Kang, J.-K., Roberts, L., 2000. Cobalt-rich ferromanganese crusts in the Pacific. In: Cronan, D.S. (Ed.), Handbook of Marine Mineral Deposits. CRC, Boca Raton, pp. 239–279.

Hein, J.R., Koschinsky, A., Halliday, A.N., 2003. Global occurrence of tellurium-rich ferromanganese crusts and a model for the enrichment of tellurium. Geochimica et Cosmochimica Acta 67, 1117–1127.

Hoffmann, J.E., Münker, C., Polat, A., König, S., Mezger, K., Rosing, M.T., 2010. Highly depleted Hadean mantle reservoirs in the sources of early Archean arc-like rocks, Isua supracrustal belt, southern West Greenland. Geochimica et Cosmochimica Acta 74, 7236–7260.

Holland, H.D., 1994. Early Proterozoic atmospheric change. In: Bengtson, S. (Ed.), Early Life on Earth. Columbia University Press, New York, pp. 237–244.

Jaun, B., Thauer, R.K., 2007. Methyl-coenzyme M reductase and its nickel Corphin coenzyme F430 in methanogenic Archaea. In: Sigel, A., Sigel, H., Sigel, R.K.O. (Eds.), Nickel and its Surprising Impact in Nature, Metal Ions in Life Sciences, vol. 2. John Wiley & Sons, Ltd, Chichester, UK, pp. 323–356.

Kato, Y., Ohta, I., Tsunematsu, T., Watanabe, Y., Isozaki, Y., Maruyama, S., Imai, N., 1998. Rare earth element variations in mid-Archean banded iron formations: implications for the chemistry of ocean and continent and plate tectonics. Geochimica et Cosmochimica Acta 62, 3475–3497.

Kato, Y., Kano, T., Kunugiza, K., 2002. Negative Ce anomaly in the Indian banded iron formations: evidence for the emergence of oxygenated deep-sea at 2.9–2.7 Ga. Resource Geology 52, 101–110.

Klein, C., 2005. Some Precambrian banded iron-formations (BIFs) from around the world: their age, geologic setting, mineralogy, metamorphism, geochemistry, and origins. American Mineralogist 90, 1473–1499.

Klinkhammer, G., German, C.R., Elderfield, H., Greaves, M.J., Mitra, A., 1994. Rare earth elements in hydrothermal fluids and plume particulates by inductively coupled plasma mass spectrometry. Marine Chemistry 45, 179–186.

Komiya, T., Maruyama, S., Masuda, T., Nohda, S., Hayashi, M., Okamoto, K., 1999. Plate tectonics at 3.8-3.7 Ga: field evidence from the Isua accretionary complex, southern West Greenland. Journal of Geology 107, 515–554.

Komiya, T., Hayashi, M., Maruyama, S., Yurimoto, H., 2002. Intermediate-P/T type Archean metamorphism of the Isua supracrustal belt: implications for secular change of geothermal gradients at subduction zones and for Archean plate tectonics. American Journal of Science 302, 804–826.

Komiya, T., Hirata, T., Kitajima, K., Yamamoto, S., Shibuya, T., Sawaki, Y., Ishikawa, T., Shu, D., Li, Y., Han, J., 2008. Evolution of the composition of seawater through geologic time, and its influence on the evolution of life. Gondwana Research 14, 159–174.

Komiya, T., Yamamoto, S., Aoki, S., Sawaki, Y., Ishikawa, A., Tashiro, T., Koshida, K., Shimojo, M., Aoki, K., Collerson, K.D., 2015. Geology of the Eoarchean, >3.95 Ga, Nulliak supracrustal rocks in the Saglek Block, northern Labrador, Canada: the oldest geological evidence for plate tectonics. Tectonophysics 662, 40–66.

Konhauser, K.O., Pecoits, E., Lalonde, S.V., Papineau, D., Nisbet, E.G., Barley, M.E., Arndt, N.T., Zahnle, K., Kamber, B.S., 2009. Oceanic nickel depletion and a methanogen famine before the Great Oxidation Event. Nature 458, 750–753.

Konhauser, K.O., Lalonde, S.V., Planavsky, N.J., Pecoits, E., Lyons, T.W., Mojzsis, S.J., Rouxel, O.J., Barley, M.E., Rosiere, C., Fralick, P.W., Kump, L.R., Bekker, A., 2011. Aerobic bacterial pyrite oxidation and acid rock drainage during the Great Oxidation Event. Nature 478, 369–373.

Liscomb, W.N., Sträter, N., 1996. Recent advances in zinc enzymology. Chemical Reviews 96, 2375–2434.

Li, Y.H., 1981. Ultimate removal mechanisms of elements from the ocean. Geochimica et Cosmochimica Acta 45, 1659–1664.

Li, Y.H., 1982. Ultimate removal mechanisms of elements from the ocean (reply to a comment by M.W Whitfield and D.R. Turner). Geochimica et Cosmochimica Acta 46, 1993–1995.

Manikyamba, C., Balaram, V., Naqvi, S.M., 1993. Geochemical signatures of polygenetic origin of a banded iron formation (BIF) of the Archaean Sandur greenstone belt (schist belt) Karnataka nucleus, India. Precambrian Research 61, 137–164.

Martin, J.-M., Whitfield, M., 1983. The significance of the river input of chemical elements to the ocean. In: Wong, C.S., Boyle, E., Bruland, K.W., Burton, J.D., Goldberg, E.D. (Eds.), Trace Metals in Sea Water, Volume 9 of the Series NATO Conference Series. Plenum Press, New York, pp. 265–296.

McGregor, V.R., Friend, C.R.L., Nutman, A.P., 1991. The late Archean mobile belt through Godthåbsfjord, southern West Greenland: a continent-continent collision zone? Bulletin of the Geological Society of Denmark 39, 179–197.

McGregor, V.R., 1993. Descriptive Text to 1:100000 Geological Map of GREENLAND Qôrqut 64 V.1 Syd. Geological Survey of Greenland, Copenhagen, 40 pp.

Mloszewska, A.M., Pecoits, E., Cates, N.L., Mojzsis, S.J., O'Neil, J., Robbins, L.J., Konhauser, K.O., 2012. The composition of Earth's oldest iron formations: the Nuvvuagittuq Supracrustal Belt (Québec, Canada). Earth and Planetary Science Letters 317–318, 331–342.

Mloszewska, A.M., Mojzsis, S.J., Pecoits, E., Papineau, D., Dauphas, N., Konhauser, K.O., 2013. Chemical sedimentary protoliths in the >3.75 Ga Nuvvuagittuq Supracrustal Belt (Québec, Canada). Gondwana Research 23, 574–594.

Mojzsis, S.J., Coath, C.D., Greenwood, J.P., McKeegan, K.D., Harrison, T.M., 2003. Mass-independent isotope effects in Archean (2.5 to 3.8 Ga) sedimentary sulfides determined by ion microprobe analysis. Geochimica et Cosmochimica Acta 67, 1635–1658.

Moorbath, S., O'Nions, R.K., Pankhurst, R.J., 1973. Early Archaean age for the Isua iron formation, west Greenland. Nature 245, 138–139.

Myers, J.S., 2001. Protoliths of the 3.8–3.7 Ga Isua greenstone belt, West Greenland. Precambrian Research 105, 129–141.

Nishizawa, M., Yamamoto, H., Ueno, Y., Tsuruoka, S., Shibuya, T., Sawaki, Y., Yamamoto, S., Kon, Y., Kitajima, K., Komiya, T., Maruyama, S., Hirata, T., 2010. Grain-scale iron isotopic distribution of pyrite from Precambrian shallow marine carbonate revealed by a femtosecond laser ablation multicollector ICP-MS technique: possible proxy for the redox state of ancient seawater. Geochimica et Cosmochimica Acta 74, 2760–2778.

Nozaki, Y., Zhang, J., Amakawa, H., 1997. The fractionation between Y and Ho in the marine environment. Earth and Planetary Science Letters 148, 329–340.

Nutman, A.P., Allaart, J.H., Bridgwater, D., Dimroth, E., Rosing, M., 1984. Stratigraphic and geochemical evidence for the depositional environment of the early Archaean Isua supracrustal belt, southern West Greenland. Precambrian Research 25, 365–396.

Nutman, A.P., 1986. The early Archaean to Proterozoic History of the Isukasia Area, Southern West Greenland, 154. Grønlands Geologiske Undersøgelse Bulletin, København, Denmark, 80 pp.

Nutman, A.P., Friend, C.R.L., Kinny, P.D., McGregor, V.R., 1993. Anatomy of an Early Archean gneiss complex: 3900 to 3600 Ma crustal evolution in southern West Greenland. Geology 21, 415–418.

Nutman, A.P., McGregor, V.R., Friend, C.R.L., Bennett, V.C., Kinny, P.D., 1996. The Itsaq Gneiss Complex of southern West Greenland; the world's most extensive record of early crustal evolution (3900–3600 Ma). Precambrian Research 78, 1–39.

Nutman, A.P., Bennett, V.C., Friend, C.R.L., Rosing, M.T., 1997a. ~ 3710 and ≥ 3790 Ma volcanic sequences in the Isua (Greenland) supracrustal belt; structural and Nd isotope implications. Chemical Geology 141, 271–287.

Nutman, A.P., Mojzsis, S., Friend, C.R.L., 1997b. Recognition of ≥3850 Ma water-lain sediments in West Greenland and their significance for the early Archaean Earth. Geochimica et Cosmochimica Acta 61, 2475–2484.

Nutman, A.P., Friend, C.R.L., Bennett, V.C., 2002. Evidence for 3650–3600 Ma assembly of the northern end of the Itsaq gneiss complex, Greenland: implication for early Archaean tectonics. Tectonics 21. http://dx.doi.org/10.1029/2000TC001203.

Nutman, A.P., Friend, C.R.L., Horie, K., Hidaka, H., 2007. The Itsaq Gneiss Complex of southern West Greenland and the construction of Eoarchaean crust at convergent plate boundaries. In: van Kranendonk, M.J., Smithies, R.H., Bennett, V.C. (Eds.), Earth's Oldest Rocks. Elsevier, Amsterdam, pp. 187–218.

Nutman, A.P., Friend, C.R.L., 2009. New 1:20,000 scale geological maps, synthesis and history of investigation of the Isua supracrustal belt and adjacent orthogneisses, southern West Greenland: a glimpse of Eoarchaean crust formation and orogeny. Precambrian Research 172, 189–211.

Nutman, A.P., Friend, C.R.L., Paxton, S., 2009. Detrital zircon sedimentary provenance ages for the Eoarchaean Isua supracrustal belt southern West Greenland: juxtaposition of an imbricated ca. 3700 Ma juvenile arc against an older complex with 3920-3760 Ma components. Precambrian Research 172, 212–233.

Nutman, A.P., Friend, C.R.L., Bennett, V.C., Wright, D., Norman, M.D., 2010. ≥3700 Ma pre-metamorphic dolomite formed by microbial mediation in the Isua

京都大学 KYOTO UNIVERSITY
A Self-archived copy in
Kyoto University Research Information Repository
https://repository.kulib.kyoto-u.ac.jp
京都大学学術情報リポジトリ KURENAI 紅 Kyoto University Research Information Repository



supracrustal belt (W. Greenland): simple evidence for early life? Precambrian Research 183, 725–737.
Olivarez, A.M., Owen, R.M., 1991. The europium anomaly of seawater: implications for fluvial versus hydrothermal REE inputs to the oceans. Chemical Geology 92, 317–328.
Partin, C.A., Lalonde, S.V., Planavsky, N.J., Bekker, A., Rouxel, O.J., Lyons, T.W., Konhauser, K.O., 2013. Uranium in iron formations and the rise of atmospheric oxygen. Chemical Geology 362, 82–90.
Pavlov, A.A., Kasting, J.F., Brown, L.L., Rages, K.A., Freedman, R., 2000. Greenhouse warming by $CH_4$ in the atmosphere of early Earth. Journal of Geophysical Research 105, 11981–11990.
Pecoits, E., Gingras, M.K., Barley, M.E., Kappler, A., Posth, N.R., Konhauser, K.O., 2009. Petrography and geochemistry of the Dales Gorge banded iron formation: paragenetic sequence, source and implications for palaeo-ocean chemistry. Precambrian Research 172, 163–187.
Planavsky, N.J., Asael, D., Hofmann, A., Reinhard, C.T., Lalonde, S.V., Knudsen, A., Wang, X., Ossa Ossa, F., Pecoits, E., Smith, A.J.B., Beukes, N.J., Bekker, A., Johnson, T.M., Konhauser, K.O., Lyons, T.W., Rouxel, O.J., 2014. Evidence for oxygenic photosynthesis half a billion years before the Great Oxidation Event. Nature Geoscience 7, 283–286.
Polat, A., Hofmann, A.W., Rosing, M., 2002. Boninite-like volcanic rocks in the 3.7-3.8 Ga Isua greenstone belt, West Greenland: geochemical evidence for intra-oceanic subduction zone processes in the early Earth. Chemical Geology 184, 231–254.
Polat, A., Hofmann, A.W., 2003. Alteration and geochemical patterns in the 3.7–3.8 Ga Isua greenstone belt, West Greenland. Precambrian Research 126, 197–218.
Polat, A., Frei, R., 2005. The origin of early Archean banded iron formations and of continental crust, Isua, southern West Greenland. Precambrian Research 138, 151–175.
Polat, A., Wang, L., Appel, P.W.U., 2015. A review of structural patterns and melting processes in the Archean craton of West Greenland: evidence for crustal growth at convergent plate margins as opposed to non-uniformitarian models. Tectonophysics 662, 67–94.
Ragdale, S.W., 2014. Biochemistry of methyl-coenzyme M reductase: the nickel Metalloenzyme that catalyzes the final step in synthesis and the first step in Anaerobic oxidation of the greenhouse gas methane. In: Kroneck, P.M.H., Sosa Torres, M.E. (Eds.), The Metal-driven Biogeochemistry of Gaseous Compounds in the Environment, Metal Ions in Life Sciences 14. Springer, pp. 125–145.
Rollinson, H., 2002. The metamorphic history of the Isua greenstone belt, West Greenland. In: Fowler, C.M.R., Ebinger, C.J., Hawkesworth, C.J. (Eds.), The Early Earth: Physical, Chemical, and Biological Development, Geological Society, London, Special Publications, 199, pp. 329–350.
Rollinson, H., 2003. Metamorphic history suggested by garnet-growth chronologies in the Isua greenstone belt, West Greenland. Precambrian Research 126, 181–196.
Rose, N.M., Rosing, M.T., Bridgwater, D., 1996. The origin of metacarbonate rocks in the Archaean Isua supracrustal belt, West Greenland. American Journal of Science 296, 1004–1044.
Rosing, M.T., Rose, N.M., Bridgwater, D., Thomsen, H.S., 1996. Earliest part of Earth's stratigraphic record: a reappraisal of the > 3.7 Ga Isua (Greenland) supracrustal sequence. Geology 24, 43–46.
Ruhlin, D.E., Owen, R.M., 1986. The rare-earth element geochemistry of hydrothermal sediments from the East Pacific Rise: exhumation of a seawater scavenging mechanism. Geochimica et Cosmochimica Acta 50, 393–400.
Sherrell, R.M., Field, M.P., Ravizza, G., 1999. Uptake and fractionation of rare earth elements on hydrothermal plume particles at 9°ã45°äN, East Pacific Rise. Geochimica et Cosmochimica Acta 63, 1709–1722.
Shimizu, H., Umemoto, N., Masuda, A., Appel, P.W.U., 1990. Sources of iron-formations in the Archean Isua and Malene supracrustals, West Greenland: evidence from La-Ce and Sm-Nd isotopic data and REE abundances. Geochimica et Cosmochimica Acta 54, 1147–1154.
Sigel, H., Sigel, A., 1995. Vanadium and its Role in Life, Metal Ions in Biological Systems, vol. 31. Marcel Dekker, Inc., New York, 779 pp.
Spear, F.S., 1993. Metamorphic Phase Equilibria and Pressure-Temperature-Time Paths. Mineralogical Society of America, Washington, D. C., 799 pp.
Swanner, E.D., Planavsky, N.J., Lalonde, S.V., Robbins, L.J., Bekker, A., Rouxel, O.J., Saito, M.A., Kappler, A., Mojzsis, S.J., Konhauser, K.O., 2014. Cobalt and marine redox evolution. Earth and Planetary Science Letters 390, 253–263.
Szilas, K., Kelemen, P.B., Rosing, M.T., 2015. The petrogenesis of ultramafic rocks in the > 3.7 Ga Isua supracrustal belt, southern West Greenland: geochemical evidence for two distinct magmatic cumulate trends. Gondwana Research 28, 565–580.
Takahashi, Y., Ariga, D., Fan, Q., Kashiwabara, T., 2015. Systematics of distributions of various elements between ferromanganese oxides and seawater from natural observation, thermodynamics, and structures. In: Ishibashi, J.-i., Okino, K., Sunamura, M. (Eds.), Subseafloor Biosphere Linked to Hydrothermal Systems: TAIGA Concept. Springer Japan, Tokyo, pp. 39–48.
Takai, K., Nakamura, K., Suzuki, K., Inagaki, F., Nealson, K.H., Kumagai, H., 2006. Ultramafics-Hydrothermalism-Hydrogenesis-HyperSLiME (UltraH3) linkage: a key insight into early microbial ecosystem in the Archean deep-sea hydrothermal systems. Paleontological Research 10, 269–282.
Taylor, S.R., McLennan, S.M., 1985. The Continental Crust: Its Composition and Evolution. Blackwell, Oxford, 312 pp.
Viehmann, S., Bau, M., Smith, A.J.B., Beukes, N.J., Dantas, E.L., Bühn, B., 2015a. The reliability of ~2.9 Ga old Witwatersrand banded iron formations (South Africa) as archives for Mesoarchean seawater: evidence from REE and Nd isotope systematics. Journal of African Earth Sciences 111, 322–334.
Viehmann, S., Bau, M., Hoffmann, J.E., Münker, C., 2015b. Geochemistry of the Krivoy Rog Banded Iron Formation, Ukline, and the impact of peak episodes of increased global magmatic activity on the trace element composition of Precambrian seawater. Precambrian Research 270, 165–180.
Whitehouse, M.J., Kamber, B.S., Fedo, C.M., Lepland, A., 2005. Integrated Pb- and S-isotope investigation of sulphide minerals from the early Archaean of southwest Greenland. Chemical Geology 222, 112–131.
Whitehouse, M.J., Fedo, C.M., 2007. Microscale heterogeneity of Fe isotopes in >3.71 Ga banded iron formation from the Isua greenstone belt, southwest Greenland. Geology 35, 719–722.
Yoshiya, K., Nishizawa, M., Sawaki, Y., Ueno, Y., Komiya, T., Yamada, K., Yoshida, N., Hirata, T., Wada, H., Maruyama, S., 2012. *In situ* iron isotope analyses of pyrite and organic carbon isotope ratios in the Fortescue Group: metabolic variations of a Late Archean ecosystem. Precambrian Research 212–213, 169–193.
Yoshiya, K., Sawaki, Y., Hirata, T., Maruyama, S., Komiya, T., 2015. *In-situ* iron isotope analysis of pyrites in ~ 3.7 Ga sedimentary protoliths from the Isua supracrustal belt, southern West Greenland. Chemical Geology 401, 126–139.